



Output-only identification of input–output models[☆]

Khaled F. Aljanaideh^{a,*}, Dennis S. Bernstein^b

^a Aeronautical Engineering Department, Jordan University of Science and Technology, Irbid, 22110, Jordan

^b Aerospace Engineering Department, University of Michigan, 1320 Beal St., Ann Arbor, MI 48109, United States of America



ARTICLE INFO

Article history:

Received 20 October 2018

Received in revised form 20 June 2019

Accepted 10 October 2019

Available online 12 November 2019

Keywords:

System identification

Output-only identification

System modeling and analysis

Transmissibility

ABSTRACT

In applications of system identification where the input signal is unknown, transmissibility identification can be used to estimate the operator between a pair of output signals. A limitation of transmissibility identification is the fact that the numerator and denominator of a transmissibility are numerators of the transfer functions from the input to the sensors. Consequently, transmissibility identification does not capture the poles of the system. To overcome this limitation, this paper introduces transmissibility-based system identification (TBSID), which uses estimates of two transmissibilities to identify the complete dynamics from two unmeasured inputs to two measured outputs. The method assumes that the system can be excited nonsimultaneously by two input signals at two distinct locations.

© 2019 Elsevier Ltd. All rights reserved.

1. Introduction

System identification uses input–output data to construct empirical input–output models (Juang, 1994; Ljung, 1998; Söderström & Stoica, 1989). For vibrational systems, the goal is to estimate the modal characteristics of the structure, including modal frequencies, damping ratios, and mode shapes (Ewins, 1984, 2000; Hermans & Van der Auweraer, 1999). In many applications, however, measurements of the response are available, but measurements of the input are not. Examples include bridges excited by vehicles as well as buildings excited by wind. In these applications, only measurements of the structural response are available.

Various techniques have been developed for identification using only sensor response data. These techniques include blind identification (Abed-Meraim, Qiu, & Hua, 1997; Moulines, Duhamel, Cardoso, & Mayrargue, 1995; Tong, Xu, & Kailath, 1994) and operational modal analysis (Brincker, Zhang, & Andersen, 2001; Devriendt & Guillaume, 2008; Peeters & De Roeck, 2001; Weijtjens, De Sitter, Devriendt, & Guillaume, 2014; Zhang, Wang,

& Tamura, 2010). Since measurements of the input are not available, most of these techniques assume that the excitation is white noise.

In the case where sensor (output) data are available from at least two sensors but actuation (input) data are not available, it is possible to estimate transmissibilities. Estimation of transmissibilities and their application to structures and acoustics has been widely studied in the frequency domain (Brincker et al., 2001; Devriendt & Guillaume, 2007, 2008; Maamar, Abdelghani, Le, Gagnol, & Sabourin, 2019). More recently, techniques for time-domain transmissibility identification have been developed (Lo, Lynch, & Liu, 2011, 2012, 2013) along with a theoretical framework for understanding the meaning of a transmissibility as an operator (Aljanaideh & Bernstein, 2015a, 2015b, 2018a). In particular, it is shown in Aljanaideh and Bernstein (2017a) that a transmissibility can be viewed within the framework of behaviors, where the transmissibility relates response signals and the unknown input is viewed as a latent variable. Time-domain analysis of transmissibilities also shows that the “dynamics” captured by a transmissibility operator correspond to the zeros of the transfer functions from the external input to the sensors. Consequently, transmissibility identification provides an estimate of the numerators of transfer functions but not their denominators.

Transmissibility-based operational modal analysis (TOMA) uses frequency-domain techniques to estimate transmissibilities (Devriendt & Guillaume, 2008; Weijtjens et al., 2014). A drawback of TOMA is that, under nonzero initial conditions, the estimates depend on the initial condition and the excitation signal acting on the underlying system. Transmissibilities identified under a given operating condition may therefore be inaccurate under other operating conditions (Aljanaideh & Bernstein, 2015b).

[☆] This research was supported in part by National Science Foundation, USA under Grant No. CMMI 1536834 and Jordan University of Science and Technology, Irbid, Jordan under Grant No. 20180304. The material in this paper was partially presented at the 57th IEEE Conference on Decision and Control, December 17–19, 2018, Miami Beach, Florida, USA. This paper was recommended for publication in revised form by Associate Editor Juan C. Aguero under the direction of Editor Torsten Söderström.

* Corresponding author.

E-mail addresses: kfaljanaideh@just.edu.jo (K.F. Aljanaideh), dsbaero@umich.edu (D.S. Bernstein).

In addition, as shown in Section 3, TOMA methods based on non-parametric frequency-domain identification can estimate only undamped or lightly damped modes. On the other hand, TOMA methods based on parametric frequency-domain identification such as Devriendt, De Sitter, and Guillaume (2010), Devriendt, De Sitter, Vanlanduit, and Guillaume (2009) and Weijtjens et al. (2014) do not consider the fact that transmissibility identification is an errors-in-variables (EIV) identification problem. Moreover, since these techniques consider a rational function model of the transmissibility (Devriendt et al., 2010, 2009; Weijtjens et al., 2014), overestimating or underestimating the order of the transmissibility may yield poor parameter estimates (Aljanaideh & Bernstein, 2017b).

To overcome these limitations, the present paper develops transmissibility-based system identification (TBSID). TBSID is a novel approach to estimating the underlying dynamics of a system in the case where only sensor response data are available. In particular, as in the case of frequency-domain transmissibility estimation (Devriendt & Guillaume, 2008; Weijtjens et al., 2014), TBSID assumes that the system can be excited nonsimultaneously by input signals at two distinct locations. Noncausal FIR models and noncausal composite FIR/IIR models are used for time-domain identification of transmissibility operators (Aljanaideh & Bernstein, 2017b, 2018d). Moreover, an EIV algorithm for transmissibility identification using noncausal FIR models is introduced. The transmissibilities arising from the inputs are identified, and these estimates are then combined to estimate the system dynamics. In the case of structural vibration, this technique provides estimates of the modal frequencies of the structure using only response data.

An advantage of TBSID is the fact that the excitation signals and their locations can be completely unknown. In fact, as long as they are sufficiently persistent and nonsimultaneous, the excitation signals can be provided by any unspecified and unknown ambient process at any pair of unspecified and unknown locations. For example, TBSID was used in Aljanaideh and Bernstein (2018c) to construct the lateral aircraft dynamics with measurements of roll-rate and yaw-rate perturbations from steady straight-line flight and without using knowledge of the control-surface deflections and thrust.

The contents of this paper are as follows. In Section 2, transmissibility operators are constructed from state space models. Section 3 reviews the classical frequency-domain-based approach of modal identification using transmissibilities, and shows a motivating example. Section 4 shows that transmissibility operators can be used to identify the dynamics and the complete input-output model of the underlying system. Section 5 shows three illustrative examples for the main result introduced in the paper. Section 6 shows that noncausal FIR models and composite noncausal FIR/IIR models can be used to identify transmissibility operators. Section 7 shows an errors-in-variables (EIV) algorithm for transmissibility identification. Section 8 shows a numerical example, and experimental results applied to acoustic systems are shown in Section 9. Finally, conclusions are given in Section 10.

Notation. Let A be an $n \times n$ matrix. Then, $A_{(i,j)}$ denotes the i, j entry of A ; $A_{[i,j]}$ denotes the $(n-1) \times (n-1)$ submatrix of A obtained by deleting the i th row and j th column of A ; and $A_{\{[i,j],\{k,l\}\}}$ denotes the $(n-2) \times (n-2)$ submatrix of A obtained by deleting the i th row, j th row, k th column, and l th column of A . $\text{mspec}(A)$ denotes the multiset of eigenvalues of A including multiplicity, $\text{mroots}(p)$ denotes the multiset of roots of the polynomial p including multiplicity, and $\text{mzeros}(\mathcal{T})$ denotes the multiset of zeros of the rational function \mathcal{T} including multiplicity.

2. Transmissibility operators

Consider the single-input, two-output system

$$\dot{x}(t) = Ax(t) + bu(t), \quad (1)$$

$$x(0) = x_0, \quad (2)$$

$$y_i(t) \triangleq c_i x(t) + d_i u(t), \quad (3)$$

$$y_o(t) \triangleq c_o x(t) + d_o u(t), \quad (4)$$

where $A \in \mathbb{R}^{n \times n}$, $b \in \mathbb{R}^n$, $c_i, c_o \in \mathbb{R}^{1 \times n}$, and $d_i, d_o \in \mathbb{R}$. The input signal u and the output signals y_i and y_o are scalar. Define the polynomials

$$\Gamma_i(\mathbf{p}) \triangleq c_i \text{adj}(\mathbf{p}I - A)b + d_i \delta(\mathbf{p}), \quad (5)$$

$$\Gamma_o(\mathbf{p}) \triangleq c_o \text{adj}(\mathbf{p}I - A)b + d_o \delta(\mathbf{p}), \quad (6)$$

$$\delta(\mathbf{p}) \triangleq \det(\mathbf{p}I - A), \quad (7)$$

where $\mathbf{p} \triangleq d/dt$, and assume that $\Gamma_i(\mathbf{p})$ is not the zero polynomial. Combining (5), (6) yields (Aljanaideh & Bernstein, 2015b)

$$\Gamma_i(\mathbf{p})y_o = \Gamma_o(\mathbf{p})y_i. \quad (8)$$

We write (8) as

$$y_o = \mathcal{T}_{c_o, c_i | b}(\mathbf{p})y_i, \quad (9)$$

where the *transmissibility operator* from y_i to y_o is defined by (Aljanaideh & Bernstein, 2015b)

$$\mathcal{T}_{c_o, c_i | b}(\mathbf{p}) \triangleq \frac{\Gamma_o(\mathbf{p})}{\Gamma_i(\mathbf{p})}. \quad (10)$$

Since division by \mathbf{p} is not defined, (9) and (10) provide a convenient but not literal representation of the time-domain relation (8). The subscript b indicates that the transmissibility operator depends on the way in which the input drives the system.

Since $\mathcal{T}_{c_o, c_i | b}$ is not the forced response of a linear system, $\mathcal{T}_{c_o, c_i | b}$ is not a transfer function in the usual sense. Moreover, note that the roots of Γ_o and Γ_i are the zeros of the transfer functions from u to y_o and u to y_i , respectively. Finally, unlike the complex Laplace variable s , the time-domain operator \mathbf{p} in (9) accounts for nonzero initial conditions as explained in Aljanaideh and Bernstein (2015b, 2018b).

3. Frequency-domain-identification-based approach

Identification of modal parameters based on frequency-domain transmissibilities was considered in Devriendt et al. (2010), Devriendt and Guillaume (2008) and Weijtjens et al. (2014), where parametric and nonparametric frequency-domain identification methods were used to estimate the modal parameters using transmissibility estimates.

As shown in Aljanaideh and Bernstein (2015b), a major drawback of frequency-domain transmissibility estimation is that under nonzero initial conditions the transmissibility estimates depend on the initial condition and the excitation signal. This implies that transmissibilities identified under a given operating conditions may be invalid under other operating conditions. Moreover, as shown in Aljanaideh, Sanjeevini, and Bernstein (2018), since both the input and output of the transmissibility are outputs of the underlying system, and real measurements of outputs are corrupted by noise, transmissibility identification is an EIV identification problem, which was not considered in the literature of TOMA. Parametric identification of transmissibilities, which was considered in Devriendt et al. (2010) and Weijtjens et al. (2014) requires knowledge of the order of the transmissibility. Since the dynamics of the underlying system are unknown,

then the order of the transmissibility is also unknown, and underestimating or overestimating the order of the transmissibility may yield erroneous estimates.

As shown in Devriendt and Guillaume (2008), the frequency response of the transmissibilities between a given pair of outputs but obtained under different loading conditions intersect at the modal frequencies of the system. Therefore, the reciprocal of the difference between these transmissibilities will have peaks at the locations of the modal frequencies of the system. However, as shown in the following example, this approach works only if the poles of the system are undamped or lightly damped.

In the following example, we use the approach introduced in Devriendt and Guillaume (2008) to estimate the modal frequencies of a system from transmissibilities. To avoid errors in the estimates of the modal frequencies due to spectral leakage or nonzero initial conditions, we construct the transmissibilities directly from the state space model instead of identifying them from output measurements using frequency-domain identification methods as in Devriendt and Guillaume (2008).

Example 3.1. Consider a continuous-time system with the state space realization (A, B, C, D) , where

$$A = \begin{bmatrix} 0 & -125 & 0 & -2500 \\ 1 & 0 & 0 & 0 \\ 0 & 1 & 0 & 0 \\ 0 & 0 & 1 & 0 \end{bmatrix}. \quad (11)$$

Then, the spectrum of A consists of the eigenvalues $\text{eig}(A) = \{\pm j5, \pm j10\}$, which are located on the imaginary axis with natural frequencies 5 rad/s and 10 rad/s. Next, suppose that

$$B = \begin{bmatrix} 1 & 0 \\ 0 & 1 \\ 1 & 1 \\ 4 & 1 \end{bmatrix}, \quad C = \begin{bmatrix} 1 & 1 & 0 & 0 \\ 1 & 0 & 0 & 1 \\ 1 & 0 & 1 & 0 \end{bmatrix}, \quad D = O_{3 \times 2}, \quad (12)$$

the input $u = [u_1 \ u_2]^T$, and the output $y = [y_1 \ y_2 \ y_3]^T$. Let $\mathcal{T}_{i,j|k}$ denote the transmissibility from y_j to y_i given that the input u_k is applied, where $i, j \in \{1, 2, 3\}$, $i \neq j$, and $k \in \{1, 2\}$. Then,

$$\mathcal{T}_{2,1|1}(\mathbf{p}) = \frac{5\mathbf{p}^3 - 9999\mathbf{p}^2 - 2000\mathbf{p} + 126}{\mathbf{p}^3 - 9999\mathbf{p}^2 - 12500\mathbf{p} - 2500}, \quad (13)$$

$$\mathcal{T}_{2,1|2}(\mathbf{p}) = \frac{\mathbf{p}^3 - 2624\mathbf{p}^2 - 2374\mathbf{p} - 2375}{\mathbf{p}^3 - 2625\mathbf{p}^2 - 5000\mathbf{p} - 5000}, \quad (14)$$

$$\mathcal{T}_{3,1|1}(\mathbf{p}) = \frac{2\mathbf{p}^3 - 10000\mathbf{p}^2 - 2374\mathbf{p} - 10000}{\mathbf{p}^3 - 9999\mathbf{p}^2 - 12500\mathbf{p} - 2500}, \quad (15)$$

$$\mathcal{T}_{3,1|2}(\mathbf{p}) = \frac{\mathbf{p}^3 - 2624\mathbf{p}^2 - 2375\mathbf{p} - 5000}{\mathbf{p}^3 - 2625\mathbf{p}^2 - 5000\mathbf{p} - 5000}. \quad (16)$$

Fig. 1 shows plots of the magnitudes of the frequency responses of $1/(\mathcal{T}_{2,1|1} - \mathcal{T}_{2,1|2})$ and $1/(\mathcal{T}_{3,1|1} - \mathcal{T}_{3,1|2})$, which have peaks at the natural frequencies of the system, that is, $\omega_{n_1} = 5$ rad/s and $\omega_{n_2} = 10$ rad/s.

Next, consider a continuous-time system with the state space realization (A, B, C, D) , where

$$A = \begin{bmatrix} -25 & -325 & -2375 & -6250 \\ 1 & 0 & 0 & 0 \\ 0 & 1 & 0 & 0 \\ 0 & 0 & 1 & 0 \end{bmatrix}. \quad (17)$$

Then, the spectrum of A consists of the eigenvalues $\text{eig}(A) = \{-5, -10, -5 \pm j10\}$, none of which are located on the imaginary axis. In particular, the system has real poles at $s = -5$ and $s = -10$ and complex-conjugate poles with a natural frequency of approximately 11.2 rad/s. Moreover, let B, C, D be given by (12), and let $u = [u_1 \ u_2]^T$ and $y = [y_1 \ y_2 \ y_3]^T$. Then,

$$\mathcal{T}_{2,1|1}(\mathbf{p}) = \frac{5\mathbf{p}^3 - 27274\mathbf{p}^2 - 4925\mathbf{p} + 9826}{\mathbf{p}^3 - 27374\mathbf{p}^2 - 33625\mathbf{p} - 6250}, \quad (18)$$

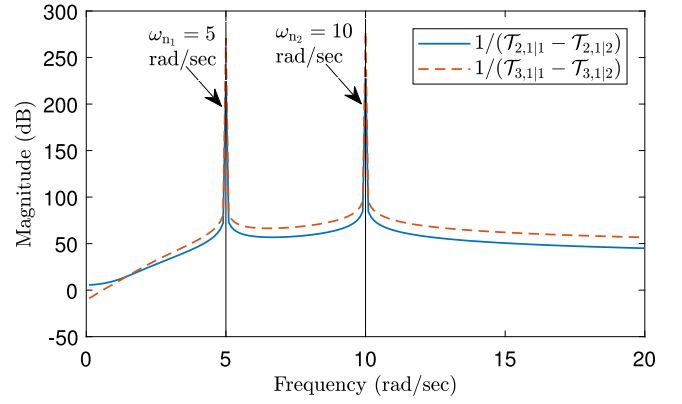


Fig. 1. Magnitude plots of the frequency responses of $1/(\mathcal{T}_{2,1|1} - \mathcal{T}_{2,1|2})$ and $1/(\mathcal{T}_{3,1|1} - \mathcal{T}_{3,1|2})$, where the poles of the system are located on the frequency axis. Note that the frequency responses of $1/(\mathcal{T}_{2,1|1} - \mathcal{T}_{2,1|2})$ and $1/(\mathcal{T}_{3,1|1} - \mathcal{T}_{3,1|2})$ have peaks at the natural frequencies of the system, that is, $\omega_{n_1} = 5$ rad/s and $\omega_{n_2} = 10$ rad/s.

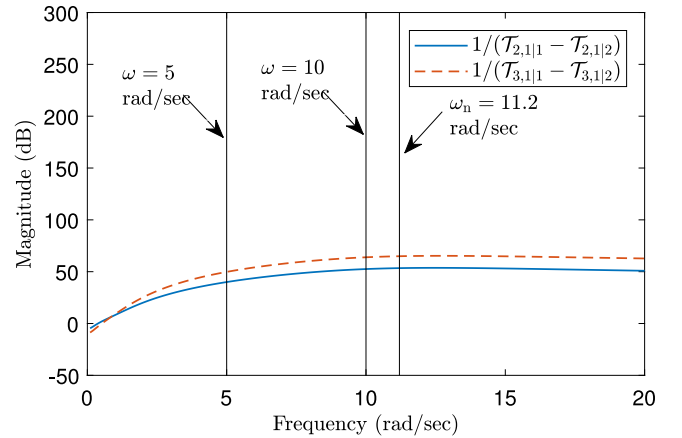


Fig. 2. Magnitude plots of the frequency responses of $1/(\mathcal{T}_{2,1|1} - \mathcal{T}_{2,1|2})$ and $1/(\mathcal{T}_{3,1|1} - \mathcal{T}_{3,1|2})$, where the poles of the system are not located on the frequency axis. Note that the frequency responses of $1/(\mathcal{T}_{2,1|1} - \mathcal{T}_{2,1|2})$ and $1/(\mathcal{T}_{3,1|1} - \mathcal{T}_{3,1|2})$ have no peaks at the frequencies of the poles of the system.

$$\mathcal{T}_{2,1|2}(\mathbf{p}) = \frac{\mathbf{p}^3 - 8924\mathbf{p}^2 - 8274\mathbf{p} - 3525}{\mathbf{p}^3 - 8925\mathbf{p}^2 - 17250\mathbf{p} - 12500}, \quad (19)$$

$$\mathcal{T}_{3,1|1}(\mathbf{p}) = \frac{2\mathbf{p}^3 - 27350\mathbf{p}^2 - 5924\mathbf{p} - 25000}{\mathbf{p}^3 - 27374\mathbf{p}^2 - 33625\mathbf{p} - 6250}, \quad (20)$$

$$\mathcal{T}_{3,1|2}(\mathbf{p}) = \frac{\mathbf{p}^3 - 8924\mathbf{p}^2 - 8275\mathbf{p} - 12500}{\mathbf{p}^3 - 8925\mathbf{p}^2 - 17250\mathbf{p} - 12500}. \quad (21)$$

Fig. 2 shows plots of the magnitudes of the frequency responses of $1/(\mathcal{T}_{2,1|1} - \mathcal{T}_{2,1|2})$ and $1/(\mathcal{T}_{3,1|1} - \mathcal{T}_{3,1|2})$, which have no peaks at the frequencies of the poles of the system. The absence of peaks shows that the nonparametric frequency-domain-identification approach fails to estimate real or highly damped poles using transmissibilities. \diamond

4. Transmissibility-based system identification (TBSID)

Let $b_1, b_2 \in \mathbb{R}^n$. Then the transmissibilities from y_i to y_o with $b = b_1$ and $b = b_2$ are given, respectively, by

$$\mathcal{T}_{c_o, c_i|b_1}(\mathbf{p}) \triangleq \frac{\Gamma_{o,1}(\mathbf{p})}{\Gamma_{i,1}(\mathbf{p})}, \quad \mathcal{T}_{c_o, c_i|b_2}(\mathbf{p}) = \frac{\Gamma_{o,2}(\mathbf{p})}{\Gamma_{i,2}(\mathbf{p})}, \quad (22)$$

where

$$\Gamma_{i,1}(\mathbf{p}) \triangleq c_i \text{adj}(\mathbf{p}I - A)b_1 + d_i \delta(\mathbf{p}), \quad (23)$$

$$\Gamma_{0,1}(\mathbf{p}) \triangleq c_0 \text{adj}(\mathbf{p}I - A)b_1 + d_0 \delta(\mathbf{p}), \tag{24}$$

$$\Gamma_{1,2}(\mathbf{p}) \triangleq c_1 \text{adj}(\mathbf{p}I - A)b_2 + d_1 \delta(\mathbf{p}), \tag{25}$$

$$\Gamma_{0,2}(\mathbf{p}) \triangleq c_0 \text{adj}(\mathbf{p}I - A)b_2 + d_0 \delta(\mathbf{p}). \tag{26}$$

Using these two transmissibilities, define

$$\begin{aligned} \Delta(\mathbf{p}) &\triangleq \begin{bmatrix} \Gamma_{1,1}(\mathbf{p}) & \Gamma_{0,1}(\mathbf{p}) \\ \Gamma_{1,2}(\mathbf{p}) & \Gamma_{0,2}(\mathbf{p}) \end{bmatrix} \\ &= \begin{bmatrix} c_1 \text{adj}(\mathbf{p}I - A)b_1 + d_1 \delta(\mathbf{p}) & c_0 \text{adj}(\mathbf{p}I - A)b_1 + d_0 \delta(\mathbf{p}) \\ c_1 \text{adj}(\mathbf{p}I - A)b_2 + d_1 \delta(\mathbf{p}) & c_0 \text{adj}(\mathbf{p}I - A)b_2 + d_0 \delta(\mathbf{p}) \end{bmatrix} \end{aligned} \tag{27}$$

and note that

$$\begin{aligned} \det \Delta(\mathbf{p}) &= \Gamma_{1,1}(\mathbf{p})\Gamma_{0,2}(\mathbf{p}) - \Gamma_{0,1}(\mathbf{p})\Gamma_{1,2}(\mathbf{p}) \\ &= c_1 \text{adj}(\mathbf{p}I - A)b_1 c_0 \text{adj}(\mathbf{p}I - A)b_2 \\ &\quad - c_0 \text{adj}(\mathbf{p}I - A)b_1 c_1 \text{adj}(\mathbf{p}I - A)b_2 \\ &\quad + \delta(\mathbf{p})(d_1 c_0 - d_0 c_1) \text{adj}(\mathbf{p}I - A)(b_2 - b_1). \end{aligned} \tag{28}$$

The following lemma, which is used in the proof of [Proposition 4.1](#), provides an expression for the determinant of a 2×2 submatrix of the adjugate of a matrix.

Lemma 1. *Let $A \in \mathbb{C}^{n \times n}$ and $i, j, k, l \in \{1, \dots, n\}$, where $i \neq k$ and $j \neq l$. Then,*

$$\begin{aligned} \det \begin{bmatrix} (\text{adj } A)_{(i,j)} & (\text{adj } A)_{(i,l)} \\ (\text{adj } A)_{(k,j)} & (\text{adj } A)_{(k,l)} \end{bmatrix} \\ = \text{sign}((k - i)(l - j))(-1)^{i+j+k+l} (\det A) \det A_{[j,l],\{i,k\}}. \end{aligned} \tag{29}$$

Proof. Using the fact that, for all $p, q \in \{1, \dots, n\}$,

$$(\text{adj } A)_{(p,q)} = (-1)^{p+q} \det A_{[q,p]},$$

it follows that

$$\begin{aligned} \det \begin{bmatrix} (\text{adj } A)_{(i,j)} & (\text{adj } A)_{(i,l)} \\ (\text{adj } A)_{(k,j)} & (\text{adj } A)_{(k,l)} \end{bmatrix} \\ = (-1)^{i+j+k+l} [(\det A_{[j,l]}) \det A_{[l,k]} - (\det A_{[j,k]}) \det A_{[l,i]}]. \end{aligned} \tag{30}$$

Next, the Jacobi identity for determinants ([Brualdi & Schneider, 1983](#), Eqn. (13)) implies

$$\begin{aligned} (\det A_{[j,i]}) \det A_{[l,k]} - (\det A_{[j,k]}) \det A_{[l,i]} \\ = \text{sign}((k - i)(l - j)) (\det A) \det A_{[j,l],\{i,k\}}. \end{aligned} \tag{31}$$

Combining (31) with (30) yields (29). \square

The following result shows that δ divides $\det \Delta$.

Proposition 4.1. *Let $n \geq 2$. Then*

$$\begin{aligned} \det \Delta(\mathbf{p}) \\ = \delta(\mathbf{p})[\varepsilon(\mathbf{p}) + (d_1 c_0 - d_0 c_1) \text{adj}(\mathbf{p}I - A)(b_2 - b_1)], \end{aligned} \tag{32}$$

where

$$\begin{aligned} \varepsilon(\mathbf{p}) &\triangleq \sum_{\substack{i,j,k,l=1 \\ i \neq k, j \neq l}}^n \text{sign}((k - i)(l - j))(-1)^{i+j+k+l} \\ &\quad \cdot c_{i,i} b_{1,j} c_{0,k} b_{2,l} \det[(\mathbf{p}I - A)_{[j,l],\{i,k\}}]. \end{aligned} \tag{33}$$

Proof. Let

$$c_i = [c_{i,1} \ \dots \ c_{i,n}] = \sum_{l=1}^n c_{i,l} e_l^T, \tag{34}$$

$$c_0 = [c_{0,1} \ \dots \ c_{0,n}] = \sum_{j=1}^n c_{0,j} e_j^T, \tag{35}$$

$$b_1 = [b_{1,1} \ \dots \ b_{1,n}]^T = \sum_{k=1}^n b_{1,k} e_k, \tag{36}$$

$$b_2 = [b_{2,1} \ \dots \ b_{2,n}]^T = \sum_{l=1}^n b_{2,l} e_l, \tag{37}$$

where for all $i \in \{1, \dots, n\}$, $e_i \in \mathbb{R}^n$ is the i th unit vector. For $i, k \in \{1, \dots, n\}$ and $j, l \in \{1, \dots, n\}$, replacing A by $\mathbf{p}I - A$ in [Lemma 1](#) yields

$$\begin{aligned} &(\text{adj}(\mathbf{p}I - A))_{(i,j)} (\text{adj}(\mathbf{p}I - A))_{(k,l)} \\ &\quad - (\text{adj}(\mathbf{p}I - A))_{(k,j)} (\text{adj}(\mathbf{p}I - A))_{(i,l)} \\ &= \text{sign}((k - i)(l - j))(-1)^{i+j+k+l} \\ &\quad \cdot \delta(\mathbf{p}) \det[(\mathbf{p}I - A)_{[j,l],\{i,k\}}]. \end{aligned} \tag{38}$$

Now, using (34)–(38) yields

$$\begin{aligned} &c_i \text{adj}(\mathbf{p}I - A)b_1 c_0 \text{adj}(\mathbf{p}I - A)b_2 \\ &\quad - c_0 \text{adj}(\mathbf{p}I - A)b_1 c_i \text{adj}(\mathbf{p}I - A)b_2 \\ &= \left(\sum_{i=1}^n c_{i,i} e_i^T \text{adj}(\mathbf{p}I - A) \sum_{j=1}^n b_{1,j} e_j \right) \\ &\quad \cdot \left(\sum_{k=1}^n c_{0,k} e_k^T \text{adj}(\mathbf{p}I - A) \sum_{l=1}^n b_{2,l} e_l \right) \\ &\quad - \left(\sum_{k=1}^n c_{0,k} e_k^T \text{adj}(\mathbf{p}I - A) \sum_{j=1}^n b_{1,j} e_j \right) \\ &\quad \cdot \left(\sum_{i=1}^n c_{i,i} e_i^T \text{adj}(\mathbf{p}I - A) \sum_{l=1}^n b_{2,l} e_l \right) \\ &= \sum_{i,j,k,l=1}^n (c_{i,i} e_i^T \text{adj}(\mathbf{p}I - A)b_{1,j} e_j) \\ &\quad \cdot (c_{0,k} e_k^T \text{adj}(\mathbf{p}I - A)b_{2,l} e_l) \\ &\quad - \sum_{i,j,k,l=1}^n (c_{0,k} e_k^T \text{adj}(\mathbf{p}I - A)b_{1,j} e_j) \\ &\quad \cdot (c_{i,i} e_i^T \text{adj}(\mathbf{p}I - A)b_{2,l} e_l) \\ &= \sum_{i,j,k,l=1}^n c_{i,i} b_{1,j} c_{0,k} b_{2,l} e_i^T \text{adj}(\mathbf{p}I - A) e_j e_k^T \text{adj}(\mathbf{p}I - A) e_l \\ &\quad - \sum_{i,j,k,l=1}^n c_{i,i} b_{1,j} c_{0,k} b_{2,l} e_k^T \text{adj}(\mathbf{p}I - A) e_j e_i^T \text{adj}(\mathbf{p}I - A) e_l \\ &= \sum_{i,j,k,l=1}^n c_{i,i} b_{1,j} c_{0,k} b_{2,l} [e_i^T \text{adj}(\mathbf{p}I - A) e_j e_k^T \\ &\quad \cdot \text{adj}(\mathbf{p}I - A) e_l - e_k^T \text{adj}(\mathbf{p}I - A) e_j e_i^T \text{adj}(\mathbf{p}I - A) e_l] \\ &= \sum_{i,j,k,l=1}^n c_{i,i} b_{1,j} c_{0,k} b_{2,l} [(\text{adj}(\mathbf{p}I - A))_{(i,j)} \\ &\quad \cdot (\text{adj}(\mathbf{p}I - A))_{(k,l)} - (\text{adj}(\mathbf{p}I - A))_{(k,j)} (\text{adj}(\mathbf{p}I - A))_{(i,l)}] \\ &= \delta(\mathbf{p}) \varepsilon(\mathbf{p}), \end{aligned} \tag{39}$$

where δ is defined by (7) and ε is defined by (33). Using (28) and (39) yields (32). \square

It follows from (28) that, if $d_1 c_0 = d_0 c_1$ and b_1 and b_2 are linearly dependent, then $\det \Delta = 0$. Assuming that $\det \Delta \neq 0$, the following theorem shows that every eigenvalue of A is a root of $\det \Delta$. Moreover, this result shows that the eigenvalues of A can be estimated using knowledge of two transmissibility operators.

Theorem 1. Assume that $\det \Delta \neq 0$. Then,

$$\text{mspec}(A) \subseteq \text{mroots}(\det \Delta) = \text{mzeros}(\mathcal{T}_{c_0, c_1|b_1} - \mathcal{T}_{c_0, c_1|b_2}). \quad (40)$$

Furthermore,

$$\text{mspec}(A) = \text{mroots}(\det \Delta) = \text{mzeros}(\mathcal{T}_{c_0, c_1|b_1} - \mathcal{T}_{c_0, c_1|b_2}) \quad (41)$$

if and only if $\deg \det \Delta = n$.

Proof. Since $\det \Delta \neq 0$, it follows from (32) that δ divides $\det \Delta$. Therefore, $\text{mspec}(A) = \text{mroots}(\delta) \subseteq \text{mroots}(\det \Delta)$, which yields the inclusion in (40). Moreover, it follows from (22) that

$$\mathcal{T}_{c_0, c_1|b_1} - \mathcal{T}_{c_0, c_1|b_2} = \frac{\Gamma_{0,1}\Gamma_{i,2} - \Gamma_{0,2}\Gamma_{i,1}}{\Gamma_{i,1}\Gamma_{i,2}} = -\frac{\det \Delta}{\Gamma_{i,1}\Gamma_{i,2}},$$

which yields the equality in (40). The last statement is immediate. \square

Theorem 1 shows that $\text{mspec}(A)$ may be a proper subset of $\text{mzeros}(\mathcal{T}_{c_0, c_1|b_1} - \mathcal{T}_{c_0, c_1|b_2})$. This means that the estimate of δ may include spurious poles. As shown in Section 6, it may be possible in practice to identify and remove these poles.

By using Theorem 1, it is possible to obtain input-output models from the unknown inputs to the sensor measurements. In particular, assuming that spurious modes are either not present or can be identified and removed, Theorem 1 shows that δ can be determined from knowledge of $\mathcal{T}_{c_0, c_1|b_1}$ and $\mathcal{T}_{c_0, c_1|b_2}$. Furthermore, since estimates of the numerators $\Gamma_{i,1}$, $\Gamma_{0,1}$, $\Gamma_{i,2}$, and $\Gamma_{0,2}$ of $G_{i,1}$, $G_{0,1}$, $G_{i,2}$, and $G_{0,2}$, respectively, are available from the estimates of $\mathcal{T}_{c_0, c_1|b_1}$ and $\mathcal{T}_{c_0, c_1|b_2}$, it follows that estimates of the transfer operators from u_1 to y_i , u_1 to y_0 , u_2 to y_i , and u_2 to y_0 can be constructed as

$$G_{i,1}(\mathbf{p}) \triangleq \frac{\Gamma_{i,1}(\mathbf{p})}{\delta(\mathbf{p})}, \quad G_{0,1}(\mathbf{p}) \triangleq \frac{\Gamma_{0,1}(\mathbf{p})}{\delta(\mathbf{p})}, \quad (42)$$

$$G_{i,2}(\mathbf{p}) \triangleq \frac{\Gamma_{i,2}(\mathbf{p})}{\delta(\mathbf{p})}, \quad G_{0,2}(\mathbf{p}) \triangleq \frac{\Gamma_{0,2}(\mathbf{p})}{\delta(\mathbf{p})}. \quad (43)$$

The complete input-output transfer operators (42) and (43) can thus be identified by using estimates of $\mathcal{T}_{c_0, c_1|b_1}$ and $\mathcal{T}_{c_0, c_1|b_2}$.

5. Illustrative examples

In the following example, the sets $\text{mspec}(A)$ and $\text{mzeros}(\mathcal{T}_{c_0, c_1|b_1} - \mathcal{T}_{c_0, c_1|b_2})$ are equal.

Example 5.1. Consider the matrix

$$A = \begin{bmatrix} 1 & 2 \\ 2 & 1 \end{bmatrix}. \quad (44)$$

Then, $\delta(\mathbf{p}) = \mathbf{p}^2 - 2\mathbf{p} - 3$, and thus $\text{mspec}(A) = \{-1, 3\}$. Letting

$$c_i = [1 \ 0], \quad c_0 = [0 \ 1], \quad (45)$$

$$b_1 = [1 \ 0]^T, \quad b_2 = [0 \ 1]^T, \quad (46)$$

it follows from (23), (26) that

$$\Gamma_{i,1} = \mathbf{p} - 1, \quad \Gamma_{0,1} = 2, \quad (47)$$

$$\Gamma_{i,2} = 2, \quad \Gamma_{0,2} = \mathbf{p} - 1. \quad (48)$$

Using (28), we have

$$\Delta(\mathbf{p}) = \begin{bmatrix} \mathbf{p} - 1 & 2 \\ 2 & \mathbf{p} - 1 \end{bmatrix},$$

and thus,

$$\det \Delta(\mathbf{p}) = \mathbf{p}^2 - 2\mathbf{p} - 3. \quad (49)$$

Since $\det \Delta = \delta$, it follows that $\text{mroots}(\det \Delta) = \{-1, 3\}$, which confirms (40). \diamond

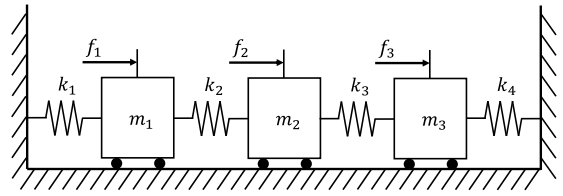


Fig. 3. Mass-spring system, where q_1 , q_2 , and q_3 are the displacements of m_1 , m_2 , and m_3 , respectively, and f_1 , f_2 , and f_3 are external forces.

In the following example, the sets $\text{mspec}(A)$ and $\text{mzeros}(\mathcal{T}_{c_0, c_1|b_1} - \mathcal{T}_{c_0, c_1|b_2})$ are not equal.

Example 5.2. Consider the matrix

$$A = \begin{bmatrix} 1 & 1 & 1 \\ 0 & 2 & -1 \\ 0 & 1 & 1 \end{bmatrix}. \quad (50)$$

Then, $\delta(\mathbf{p}) = \mathbf{p}^3 - 4\mathbf{p}^2 + 6\mathbf{p} - 3$, and thus $\text{mspec}(A) = \{1, \frac{1}{2} \pm \frac{\sqrt{3}}{2}j\}$. Letting

$$c_i = [1 \ 2 \ -1], \quad c_0 = [-1 \ 3 \ -2], \quad (51)$$

$$b_1 = [0 \ 1 \ 0]^T, \quad b_2 = [0 \ 1 \ -1]^T, \quad (52)$$

it follows from (23), (26) that

$$\Gamma_{i,1} = 2\mathbf{p}^2 - 4\mathbf{p} + 3, \quad \Gamma_{0,1} = 3\mathbf{p}^2 - 9\mathbf{p} + 5, \quad (53)$$

$$\Gamma_{i,2} = 3\mathbf{p}^2 - 6\mathbf{p} + 6, \quad \Gamma_{0,2} = 5\mathbf{p}^2 - 11\mathbf{p} + 3. \quad (54)$$

Using (28), we have

$$\Delta(\mathbf{p}) = \begin{bmatrix} 2\mathbf{p}^2 - 4\mathbf{p} + 3 & 3\mathbf{p}^2 - 9\mathbf{p} + 5 \\ 3\mathbf{p}^2 - 6\mathbf{p} + 6 & 5\mathbf{p}^2 - 11\mathbf{p} + 3 \end{bmatrix},$$

and thus,

$$\det \Delta(\mathbf{p}) = \mathbf{p}^4 + 3\mathbf{p}^3 - 22\mathbf{p}^2 + 39\mathbf{p} - 21. \quad (55)$$

Noting that $\det \Delta(\mathbf{p}) = \delta(\mathbf{p})(\mathbf{p} + 7)$, it follows that

$$\begin{aligned} \text{mspec}(A) &= \{1, \frac{1}{2} \pm \frac{\sqrt{3}}{2}j\} \subset \text{mroots}(\det \Delta) \\ &= \{1, -7, \frac{1}{2} \pm \frac{\sqrt{3}}{2}j\}, \end{aligned} \quad (56)$$

which confirms (40). Note that $\deg \delta = 3 < \deg \det \Delta = 4$. Accordingly, $\text{mroots}(\det \Delta)$ contains one spurious root, namely, -7 , and thus $\text{mspec}(A)$ is a proper subset of $\text{mroots}(\det \Delta)$. \diamond

Example 5.3. Consider the mass-spring system shown in Fig. 3 with external forces f_1, f_2, f_3 . We consider three cases, where, in each case, only one external force is nonzero. We first consider the case where $f_2 = f_3 = 0$ and $u = f_1$.

Then (1) holds with

$$x \triangleq [q_1 \ q_2 \ q_3 \ \dot{q}_1 \ \dot{q}_2 \ \dot{q}_3]^T, \quad A \triangleq \begin{bmatrix} 0_{3 \times 3} & I_3 \\ \Omega & 0_{3 \times 3} \end{bmatrix}, \quad (57)$$

$$\Omega \triangleq -M^{-1}K = \begin{bmatrix} -\frac{k_1+k_2}{m_1} & \frac{k_2}{m_1} & 0 \\ \frac{k_2}{m_2} & -\frac{k_2+k_3}{m_2} & \frac{k_3}{m_2} \\ 0 & \frac{k_3}{m_3} & -\frac{k_3+k_4}{m_3} \end{bmatrix}, \quad (58)$$

$$b = b_1 \triangleq [0 \ 0 \ 0 \ \frac{1}{m_1} \ 0 \ 0]^T, \quad u \triangleq f_1. \quad (59)$$

Moreover, define

$$q_{1,1} \triangleq y_i = c_i \text{adj}(\mathbf{p}I - A)b_1, \quad (60)$$

$$q_{3,1} \triangleq y_0 = c_0 \text{adj}(\mathbf{p}I - A)b_1, \quad (61)$$

where

$$c_i \triangleq [1 \ 0 \ 0 \ 0 \ 0 \ 0], \quad c_o \triangleq [0 \ 0 \ 1 \ 0 \ 0 \ 0]. \quad (62)$$

Then

$$\Gamma_{i,1}(\mathbf{p}) = \frac{m_2 m_3 \mathbf{p}^4 + a_1 \mathbf{p}^2 + a_0}{m_1 m_2 m_3}, \quad \Gamma_{o,1}(\mathbf{p}) = \frac{k_2 k_3}{m_1 m_2 m_3}, \quad (63)$$

where

$$a_0 \triangleq k_2 k_3 + k_2 k_4 + k_3 k_4, \quad (64)$$

$$a_1 \triangleq (k_3 + k_4)m_2 + (k_2 + k_3)m_3, \quad (65)$$

and the corresponding transmissibility operator is

$$\mathcal{T}_{c_o, g_1 | b_1}(\mathbf{p}) = \frac{\Gamma_{o,1}(\mathbf{p})}{\Gamma_{i,1}(\mathbf{p})} = \frac{k_2 k_3}{m_2 m_3 \mathbf{p}^4 + a_1 \mathbf{p}^2 + a_0}. \quad (66)$$

Next, consider the case where $f_1 = f_3 = 0$ and $u = f_2$. Then (1) holds with (57), (58), $b = b_2 = [0 \ 0 \ 0 \ 0 \ \frac{1}{m_2} \ 0]^T$, and $u = f_2$. Then

$$\Gamma_{i,2}(\mathbf{p}) = \frac{k_2 m_3 \mathbf{p}^2 + k_2 k_3 + k_2 k_4}{m_1 m_2 m_3}, \quad (67)$$

$$\Gamma_{o,2}(\mathbf{p}) = \frac{k_3 m_1 \mathbf{p}^2 + k_1 k_3 + k_2 k_3}{m_1 m_2 m_3}, \quad (68)$$

and the corresponding transmissibility operator is

$$\mathcal{T}_{c_o, g_1 | b_2}(\mathbf{p}) = \frac{\Gamma_{o,2}(\mathbf{p})}{\Gamma_{i,2}(\mathbf{p})} = \frac{k_3 m_1 \mathbf{p}^2 + k_1 k_3 + k_2 k_3}{k_2 m_3 \mathbf{p}^2 + k_2 k_3 + k_2 k_4}. \quad (69)$$

Finally, consider the case where $f_1 = f_2 = 0$ and $u = f_3$. Then (1) holds with (57), (58), $b = b_3 = [0 \ 0 \ 0 \ 0 \ 0 \ \frac{1}{m_3}]^T$, and $u = f_3$. Then

$$\Gamma_{i,3}(\mathbf{p}) = \frac{k_2 k_3}{m_1 m_2 m_3}, \quad \Gamma_{o,3}(\mathbf{p}) = \frac{m_1 m_2 \mathbf{p}^4 + c_1 \mathbf{p}^2 + c_0}{m_1 m_2 m_3}, \quad (70)$$

where

$$c_0 \triangleq k_1 k_2 + k_1 k_3 + k_2 k_3, \quad (71)$$

$$c_1 \triangleq (k_2 + k_3)m_1 + (k_1 + k_2)m_2, \quad (72)$$

and the corresponding transmissibility operator is

$$\mathcal{T}_{c_o, g_1 | b_3}(\mathbf{p}) = \frac{\Gamma_{o,3}(\mathbf{p})}{\Gamma_{i,3}(\mathbf{p})} = \frac{m_1 m_2 \mathbf{p}^4 + c_1 \mathbf{p}^2 + c_0}{k_2 k_3}. \quad (73)$$

Now, we consider Theorem 1 in all three cases. First, using (63) and (68) we have

$$\Delta(\mathbf{p}) = \begin{bmatrix} \Gamma_{i,1}(\mathbf{p}) & \Gamma_{o,1}(\mathbf{p}) \\ \Gamma_{i,2}(\mathbf{p}) & \Gamma_{o,2}(\mathbf{p}) \end{bmatrix}, \quad (74)$$

and thus

$$\det \Delta(\mathbf{p}) = \Gamma_{i,1}(\mathbf{p})\Gamma_{o,2}(\mathbf{p}) - \Gamma_{o,1}(\mathbf{p})\Gamma_{i,2}(\mathbf{p}) = \frac{k_2}{m_1 m_2 m_3} \delta(\mathbf{p}), \quad (75)$$

where

$$\delta(\mathbf{p}) = d_3 \mathbf{p}^6 + d_2 \mathbf{p}^4 + d_1 \mathbf{p}^2 + d_0, \quad (76)$$

with the coefficients

$$d_3 \triangleq \frac{k_2}{m_1 m_2 m_3}, \quad (77)$$

$$d_2 \triangleq \frac{k_2(k_3 + k_4)}{m_1 m_2 m_3^2} + \frac{k_2(k_1 m_2 + k_2 m_1 + k_2 m_2 + k_3 m_1)}{m_1^2 m_2^2 m_3}, \quad (78)$$

$$d_1 \triangleq \frac{k_2(k_1 k_2 + k_1 k_3 + k_2 k_3)}{m_1^2 m_2^2 m_3} - \frac{k_2 k_3^2}{m_1 m_2^2 m_3^2} \quad (79)$$

$$+ \frac{k_2(k_3 + k_4)(k_1 m_2 + k_2 m_1 + k_2 m_2 + k_3 m_1)}{m_1^2 m_2^2 m_3^2}, \quad (80)$$

$$d_0 \triangleq \frac{k_2(k_3 + k_4)(k_1 k_2 + k_1 k_3 + k_2 k_3) - k_2 k_3(k_1 k_3 + k_2 k_3)}{m_1^2 m_2^2 m_3^2}.$$

Therefore, $\text{mroots}(\det \Delta(\mathbf{p})) = \text{mspec}(A)$.

Next, using (63) and (70), we have

$$\Delta(\mathbf{p}) = \begin{bmatrix} \Gamma_{i,1}(\mathbf{p}) & \Gamma_{o,1}(\mathbf{p}) \\ \Gamma_{i,3}(\mathbf{p}) & \Gamma_{o,3}(\mathbf{p}) \end{bmatrix}, \quad (81)$$

and thus

$$\det \Delta(\mathbf{p}) = \Gamma_{i,1}(\mathbf{p})\Gamma_{o,3}(\mathbf{p}) - \Gamma_{o,1}(\mathbf{p})\Gamma_{i,3}(\mathbf{p}) = \frac{m_2 \mathbf{p}^2 + k_2 + k_3}{m_1 m_2 m_3} \delta(\mathbf{p}). \quad (82)$$

Therefore, $\text{mspec}(A) \subset \text{mroots}(\det \Delta(\mathbf{p}))$.

Finally, using (68) and (70) we have

$$\Delta(\mathbf{p}) = \begin{bmatrix} \Gamma_{i,2}(\mathbf{p}) & \Gamma_{o,2}(\mathbf{p}) \\ \Gamma_{i,3}(\mathbf{p}) & \Gamma_{o,3}(\mathbf{p}) \end{bmatrix}, \quad (83)$$

and thus

$$\det \Delta(\mathbf{p}) = \Gamma_{i,2}(\mathbf{p})\Gamma_{o,3}(\mathbf{p}) - \Gamma_{o,2}(\mathbf{p})\Gamma_{i,3}(\mathbf{p}) = \frac{k_3}{m_1 m_2 m_3} \delta(\mathbf{p}). \quad (84)$$

Therefore, $\text{mspec}(A) = \text{mroots}(\det \Delta(\mathbf{p}))$.

Consequently, in two of the three cases, $\text{mspec}(A)$ is equal to $\text{mroots}(\det \Delta)$, whereas, in the remaining case, $\text{mspec}(A)$ is a proper subset of $\text{mroots}(\det \Delta)$. \diamond

The transmissibility operators derived in Section 2 are formulated in continuous time. These derivations are equally valid in discrete time, where the differentiation operator \mathbf{p} is replaced by the forward-shift operator \mathbf{q} (Middleton & Goodwin, 1990). Henceforth, to facilitate applications with sampled data, we assume that measurements of the output signals are obtained in discrete time, and thus we henceforth consider discrete-time transmissibilities.

6. Estimation of transmissibility operators

Since transmissibility operators may be unstable, noncausal, and have unknown order (Aljanaideh & Bernstein, 2018a), noncausal FIR models and noncausal composite FIR/IIR (CFI) models are useful for approximation and identification of transmissibility operators. This section briefly reviews these techniques. First, we discuss noncausal FIR models (Aljanaideh & Bernstein, 2017b), and then consider noncausal CFI models (Aljanaideh & Bernstein, 2018d). Noncausal CFI models are then used to approximate transmissibility operators.

6.1. Using noncausal FIR models to approximate transmissibilities

A noncausal FIR model of \mathcal{T} is a truncation of the Laurent expansion of \mathcal{T} in an annulus that contains the unit circle. Let $\mathbb{A}(\rho_1, \rho_2)$ be the open annulus in the complex plane centered at the origin with inner radius ρ_1 and outer radius ρ_2 , where \mathcal{T} is analytic in $\mathbb{A}(\rho_1, \rho_2)$ and $\rho_1 < 1 < \rho_2$. Then, the Laurent expansion of \mathcal{T} in $\mathbb{A}(\rho_1, \rho_2)$ is given by

$$\mathcal{T}(z) = \sum_{i=-\infty}^{\infty} H_i z^{-i}, \quad (85)$$

where, for all $i \in \mathbb{Z}$, H_i is the i th coefficient of the Laurent expansion of \mathcal{T} in $\mathbb{A}(\rho_1, \rho_2)$. Therefore, an approximate noncausal FIR model of \mathcal{T} is given by

$$\mathcal{T}(\mathbf{q}, \theta_{r,d}) \triangleq \sum_{i=-d}^r H_i \mathbf{q}^{-i}, \quad (86)$$

where \mathbf{q} is the forward-shift operator and

$$\theta_{r,d} \triangleq [H_{-d} \ \cdots \ H_r] \in \mathbb{R}^{1 \times (r+d+1)}. \quad (87)$$

However, if \mathcal{T} has poles on the unit circle, then the Laurent expansion coefficients of \mathcal{T} in each annulus are bounded away from zero (Aljanaideh & Bernstein, 2017b). To overcome this difficulty, composite FIR/IIR (CFI) models can be used to approximate systems with poles on the unit circle (Aljanaideh & Bernstein, 2018d).

6.2. Using composite noncausal FIR/IIR models to approximate transmissibilities

Note that \mathcal{T} can be written as

$$\mathcal{T}(\mathbf{q}) = \frac{(\mathbf{q} - z_1) \cdots (\mathbf{q} - z_m)}{(\mathbf{q} - p_1) \cdots (\mathbf{q} - p_n)}, \quad (88)$$

where n is the order of \mathcal{T} , $z_1, \dots, z_m \in \mathbb{C}$ are the zeros of \mathcal{T} , and $p_1, \dots, p_n \in \mathbb{C}$ are the poles of \mathcal{T} . Let $l \in \{0, \dots, n\}$ be the number of poles of \mathcal{T} located on the unit circle. Hence, for all $i = 1, \dots, n-l$, $|p_i| \neq 1$, and, in the case where $l \geq 1$, for all $i = n-l+1, \dots, n$, $|p_i| = 1$. Then, define

$$D_{l,i}(\mathbf{q}) \triangleq (\mathbf{q} - p_{n-l+1}) \cdots (\mathbf{q} - p_n) = \mathbf{q}^l + \sum_{i=1}^{l-1} c_i \mathbf{q}^i, \quad (89)$$

where $c_1, \dots, c_l \in \mathbb{R}$. Then \mathcal{T} can be written as

$$\mathcal{T}(\mathbf{q}) = \frac{1}{D_{l,i}(\mathbf{q})} \mathcal{T}_l(\mathbf{q}), \quad (90)$$

where

$$\mathcal{T}_l(\mathbf{q}) \triangleq \frac{(\mathbf{q} - z_1) \cdots (\mathbf{q} - z_m)}{(\mathbf{q} - p_1) \cdots (\mathbf{q} - p_{n-l})}, \quad (91)$$

and $n-l-m$ is the relative degree of \mathcal{T}_l . Note that all of the poles of \mathcal{T}_l are either in the open unit disk or outside the closed unit disk.

Let $\mathbb{A}(\rho_1, \rho_2) \triangleq \{z \in \mathbb{C} : \rho_1 < |z| < \rho_2\}$ denote the open punctured plane centered at the origin with inner radius $0 \leq \rho_1 < 1$ and outer radius $1 \leq \rho_2$. Then, the Laurent expansion of \mathcal{T}_l in $\mathbb{A}(\rho_1, \rho_2)$ is given by

$$\mathcal{T}_l(z) = \sum_{i=-\infty}^{\infty} h_i z^{-i}, \quad (92)$$

where for all $i \in \mathbb{Z}$, $h_i \in \mathbb{R}$. Using (90) and (92) implies that, for all $z \in \mathbb{A}(\rho_1, \rho_2)$,

$$\mathcal{T}(z) = \frac{1}{D_{l,i}(z)} \sum_{i=-\infty}^{\infty} h_i z^{-i}. \quad (93)$$

Truncating the series in (93) yields the truncated model

$$\mathcal{T}_{l,r,d}(\mathbf{q}) \triangleq \frac{1}{D_{l,i}(\mathbf{q})} \mathcal{T}_{F,l,r,d}(\mathbf{q}), \quad (94)$$

where the noncausal FIR truncation $\mathcal{T}_{F,l,r,d}$ of \mathcal{T}_l is defined by

$$\mathcal{T}_{F,l,r,d}(\mathbf{q}) \triangleq \sum_{i=-d}^r h_i \mathbf{q}^{-i}. \quad (95)$$

Next, for all $k \geq 0$, let $y_i(k)$ and $y_o(k)$ be the pseudo input and pseudo output of \mathcal{T} at step k , respectively, and let ℓ denote the size of the data window.

6.3. Identification using least squares with noncausal FIR models

The least-squares estimate $\hat{\theta}_{r,d}^{\text{LS}}$ of $\theta_{r,d}$ satisfies

$$\hat{\theta}_{r,d}^{\text{LS}} = \arg \min_{\bar{\theta}_{r,d} \in \mathbb{R}^{1 \times (r+d+1)}} \|\Psi_{y_o,r,d,\ell} - \bar{\theta}_{r,d} \Phi_{y_i,r,d,\ell}\|_2, \quad (96)$$

where ℓ is the number of samples of each signal and

$$\Psi_{y_o,r,d,\ell} \triangleq [y_o(r) \ \cdots \ y_o(\ell-d)], \quad (97)$$

$$\Phi_{y_i,r,d,\ell} \triangleq [\phi_{y_i,r,d}(r) \ \cdots \ \phi_{y_i,r,d}(\ell-d)], \quad (98)$$

$$\phi_{y_i,r,d}(k) \triangleq [y_i(k+d) \ \cdots \ y_i(k-r)]^T. \quad (99)$$

It follows from (96) that the least-squares estimate $\hat{\theta}_{r,d}^{\text{LS}}$ of $\theta_{r,d}$ satisfies

$$\Psi_{y_o,r,d,\ell} \Phi_{y_i,r,d,\ell}^T = \hat{\theta}_{r,d}^{\text{LS}} \Phi_{y_i,r,d,\ell} \Phi_{y_i,r,d,\ell}^T. \quad (100)$$

As shown in Eykhoff (1974, Chapter 6), the least-squares estimate may be biased.

6.4. Identification using least squares with noncausal CFI models

Let $\theta_{l,r,d} \in \mathbb{R}^{1 \times (l+r+d)}$ denote the vector of parameters of the truncated model $\mathcal{T}_{l,r,d}$ defined by (94), where

$$\theta_{l,r,d} = [\theta_{c,l} \ \theta_{h,r,d}], \quad (101)$$

$$\theta_{c,l} = [c_1 \ \cdots \ c_{l-1}], \quad (102)$$

$$\theta_{h,r,d} = [h_{-d} \ \cdots \ h_r]. \quad (103)$$

The least squares estimate $\hat{\theta}_{l,r,d,\ell}$ of $\theta_{l,r,d}$ is given by

$$\hat{\theta}_{l,r,d,\ell} = \arg \min_{\bar{\theta}_{l,r,d} \in \mathbb{R}^{1 \times (l+r+d)}} \|\Psi_{y_o,r,d,\ell} - \bar{\theta}_{l,r,d} \Phi_{l,r,d,\ell}\|_F, \quad (104)$$

where the components of $\hat{\theta}_{l,r,d,\ell}$ are the coefficients of the noncausal CFI model (94) given by

$$\hat{\theta}_{l,r,d,\ell} = [\hat{\theta}_{c,l,r,d,\ell} \ \hat{\theta}_{h,l,r,d,\ell}],$$

$$\hat{\theta}_{c,l,r,d,\ell} = [\hat{c}_{1,\ell} \ \cdots \ \hat{c}_{l-1,\ell}],$$

$$\hat{\theta}_{h,l,r,d,\ell} = [\hat{h}_{-d,\ell} \ \cdots \ \hat{h}_{r,\ell}],$$

$$\Psi_{y_o,r,d,\ell} \triangleq [y_o(r+l) \ \cdots \ y_o(\ell-d+l)],$$

$$\Phi_{l,r,d,\ell} \triangleq \begin{bmatrix} \Phi_{y_o,l,\ell} \\ \Phi_{y_i,r,d,\ell} \end{bmatrix},$$

$$\Phi_{y_o,l,\ell} \triangleq [\phi_{y_o,l}(r) \ \cdots \ \phi_{y_o,l}(\ell-d)],$$

$$\Phi_{y_i,r,d,\ell} \triangleq [\phi_{y_i,r,d}(r+d) \ \cdots \ \phi_{y_i,r,d}(\ell)],$$

$$\phi_{y_o,l}(k) = [-y_o(k+1) \ \cdots \ -y_o(k+l-1)]^T,$$

$$\phi_{y_i,r,d}(k) = [y_i(k) \ \cdots \ y_i(k-r-d)]^T.$$

6.5. Constructing an IIR model from the identified transmissibilities

In order to construct an IIR model of a transmissibility based on an approximate noncausal FIR model, we separately estimate the asymptotically stable and unstable parts of the transmissibility using the eigensystem realization algorithm (ERA) (Juang, 1994). Then, we obtain an IIR model of the transmissibility by combining the estimates of the asymptotically stable and unstable IIR parts of the transmissibility. By choosing sufficiently large model orders n_s of the stable component and n_u of the unstable component of the transmissibility, we overestimate the orders of the stable and unstable parts of the transmissibility. Methods based on nuclear norm minimization can be used to estimate

the orders of the stable and unstable components of the transmissibility from the estimated Markov parameters (Aljanaideh & Bernstein, 2017b; Recht, Fazel, & Parrilo, 2010; Smith, 2014).

To construct an IIR model of a transmissibility based on an approximate noncausal CFI model, we first estimate an IIR model of the noncausal FIR part of the noncausal CFI model, which is then multiplied by the estimated IIR part of the noncausal CFI model.

7. Errors-in-variables identification of transmissibilities

In this section we consider EIV identification of transmissibilities using least squares with noncausal FIR models.

For EIV identification we use a modified version of the algorithm considered in Diversi (2008). The main difference between the algorithm we use in this paper and the algorithm in Diversi (2008) is that we use a noncausal FIR model to identify an IIR transmissibility operator instead of using an FIR model to identify an FIR system.

7.1. Assumptions

Suppose that both y_i and y_o are corrupted with additive white noise, that is,

$$\hat{y}_i(k) = y_i(k) + v(k), \quad (105)$$

$$\hat{y}_o(k) = y_o(k) + w(k), \quad (106)$$

where \hat{y}_i and \hat{y}_o are measurements of y_i and y_o , respectively, and v and w represent sensor noise.

We consider the following assumptions

- (A1) y_i is a realization of a zero-mean ergodic random process that is persistently exciting of a sufficient order.
- (A2) v and w are realizations of zero-mean ergodic white random processes with unknown variances.
- (A3) v and w are realizations of mutually uncorrelated random processes and are uncorrelated with the random process producing the realization y_i .

7.2. EIV identification algorithm

Here we list the steps of the algorithm. The reader can refer to Diversi (2008) for more details.

- (1) Compute $\Phi_{\hat{y}_i, r, d, \ell} \Phi_{\hat{y}_i, r, d, \ell}^T$ and $\Psi_{\hat{y}_o, r, d, \ell} \Phi_{\hat{y}_i, r, d, \ell}^T$.
- (2) Use (100) to compute the least squares estimate $\hat{\theta}_{r, d, \ell}^{LS}$.
- (3) Set $\hat{\theta}_{r, d, \ell, i}^{EIV} = \hat{\theta}_{r, d, \ell}^{LS}$, where, for all $i \geq 1$,

$$\hat{\theta}_{r, d, \ell, i}^{EIV} \triangleq [\hat{H}_{i, -d, \ell} \quad \cdots \quad \hat{H}_{i, r, \ell}], \quad (107)$$

and for all $j = -d, \dots, r$, $\hat{H}_{i, j, \ell}$ is an estimate of H_j obtained from the i th iteration of the algorithm using ℓ samples of \hat{y}_i and \hat{y}_o .

- (4) Construct the vector

$$\mathcal{H}(\hat{\theta}_{r, d, \ell, i}^{EIV}) \triangleq \begin{bmatrix} \sum_{j=-d}^{r-1} \hat{H}_{i, j, \ell} \hat{H}_{i, j+1, \ell} \\ \sum_{j=-d}^{r-2} \hat{H}_{i, j, \ell} \hat{H}_{i, j+2, \ell} \\ \vdots \\ \hat{H}_{i, -d, \ell} \hat{H}_{i, r, \ell} \end{bmatrix}. \quad (108)$$

- (5) For all $k \geq r$, compute

$$E_{r, d, \ell}(k) \triangleq \hat{y}_o(k) - \hat{\theta}_{r, d, \ell, i}^{EIV} \Phi_{\hat{y}_i, r, d, \ell}(k). \quad (109)$$

- (6) Construct

$$\mathcal{E}_{r, d, \ell} \triangleq \frac{1}{\ell} [\Psi_{E, r, d, \ell, 0} \Psi_{E, r, d, \ell, 1}^T \quad \cdots \quad \Psi_{E, r, d, \ell, 0} \Psi_{E, r, d, \ell, r+d}^T]^T, \quad (110)$$

where, for all $j = 1, \dots, r + d$,

$$\Psi_{E, r, d, \ell, j} \triangleq [E(2r + d - j) \quad \cdots \quad E(\ell - j)], \quad (111)$$

- (7) Compute

$$\hat{\sigma}_{v, r, d, \ell, i}^2 = \frac{\mathcal{H}(\hat{\theta}_{r, d, \ell, i}^{EIV})^T \mathcal{E}_{r, d, \ell}}{\mathcal{H}(\hat{\theta}_{r, d, \ell, i}^{EIV})^T \mathcal{H}(\hat{\theta}_{r, d, \ell, i}^{EIV})}. \quad (112)$$

- (8) Compute

$$\hat{\theta}_{r, d, \ell, i+1}^{EIV} = \hat{\theta}_{r, d, \ell}^{LS} + \hat{\sigma}_{v, r, d, \ell, i}^2 \hat{\theta}_{r, d, \ell, i}^{EIV} (\Phi_{\hat{y}_i, r, d, \ell} \Phi_{\hat{y}_i, r, d, \ell}^T)^{-1}. \quad (113)$$

- (9) Set $\hat{\theta}_{r, d, \ell, i}^{EIV} = \hat{\theta}_{r, d, \ell, i+1}^{EIV}$ and go to step (4).

- (10) Repeat steps (4)–(9) until

$$\frac{\|\hat{\theta}_{r, d, \ell, i+1}^{EIV} - \hat{\theta}_{r, d, \ell, i}^{EIV}\|}{\|\hat{\theta}_{r, d, \ell, i+1}^{EIV}\|} < \epsilon, \quad (114)$$

where ϵ is a predetermined convergence threshold.

8. A numerical example

This section shows a numerical example on TBSID, where output measurements that are corrupted by noise are used to identify the entire dynamics of a system.

Example 8.1. Consider the state space model

$$A = \begin{bmatrix} -0.7000 & 0.2300 & 0.2390 & 0.0546 \\ 1 & 0 & 0 & 0 \\ 0 & 1 & 0 & 0 \\ 0 & 0 & 1 & 0 \end{bmatrix}, \quad B = \begin{bmatrix} 1 & 0 \\ 1 & 0 \\ 4 & 1 \\ 0 & 1 \end{bmatrix}, \quad (115)$$

$$C = \begin{bmatrix} 1 & 2 & 3 & 0 \\ 8 & 1 & 1 & 0 \\ 1 & 3 & 1 & 6 \end{bmatrix}, \quad D = 0_{3 \times 2}. \quad (116)$$

The input is $u = [u_1 \ u_2]^T$ and the output is $y \triangleq [y_1 \ y_2 \ y_3]^T$.

We first consider the case where u_1 is a realization of a zero-mean, white, Gaussian random process with unit variance and $u_2 = 0$. We apply least squares identification with noncausal FIR models with $r = d = 25$ to estimate the Markov parameters of the transmissibilities $\mathcal{T}_{2,1|1}$ from y_1 to y_2 and $\mathcal{T}_{3,2|1}$ from y_2 to y_3 , where y_1, y_2 , and y_3 are corrupted with zero-mean white Gaussian noise with SNR values of 100 and 10. The estimated Markov parameters obtained using least squares with $r = d = 25$ are averaged over 500 independent runs of the experiment with $\ell = 50,000$ samples for each run. Then, the averaged Markov parameters are used in the EIV algorithm shown in Section 6 with $\epsilon = 10^{-8}$ to obtain the corrected Markov parameters.

Next, we consider the case where $u_1 = 0$ and u_2 is a realization of a zero-mean, white, Gaussian random process with unit variance. We apply least squares identification with noncausal FIR models with $r = d = 25$ to estimate the Markov parameters of the transmissibilities $\mathcal{T}_{2,1|2}$ from y_1 to y_2 and $\mathcal{T}_{3,2|2}$ from y_2 to y_3 , where y_1, y_2 , and y_3 are corrupted with zero-mean white Gaussian noise with SNR values of 100 and 10. The estimated Markov parameters obtained using least squares with $r = d = 25$ are averaged over 500 independent runs of the experiment with $\ell = 50,000$ samples for each run. Then, the averaged Markov

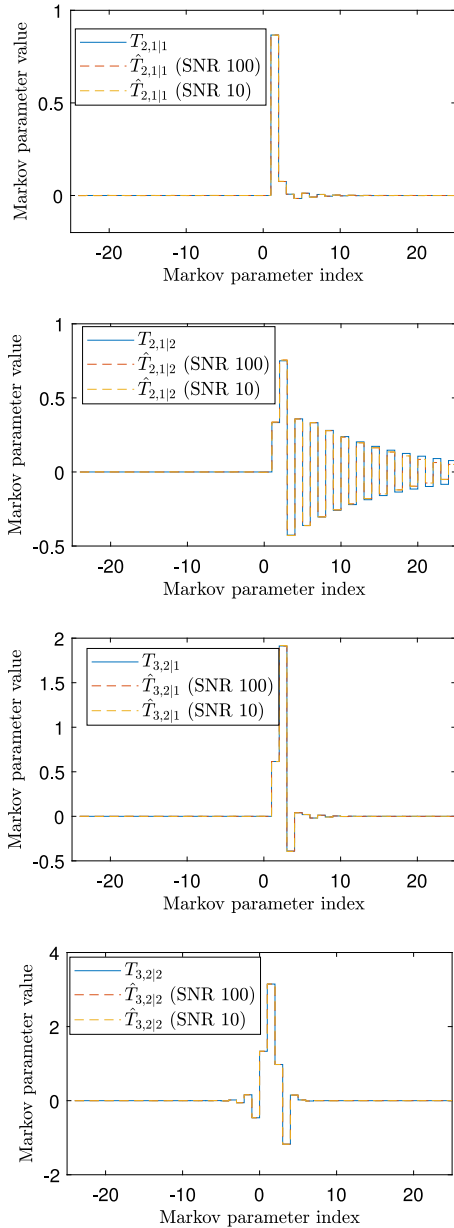


Fig. 4. Markov parameters of the transmissibilities $\mathcal{T}_{2,1|1}$, $\mathcal{T}_{2,1|2}$, $\mathcal{T}_{3,2|1}$, and $\mathcal{T}_{3,2|2}$, and estimated Markov parameters of the transmissibilities $\hat{\mathcal{T}}_{2,1|1}$, $\hat{\mathcal{T}}_{2,1|2}$, $\hat{\mathcal{T}}_{3,2|1}$, and $\hat{\mathcal{T}}_{3,2|2}$ obtained using the EIV algorithm shown in Section 6. The least squares estimate of the Markov parameters, which is used in the EIV algorithm, is obtained with a noncausal FIR model with $r = d = 25$ and $\ell = 50,000$ samples, and averaged over 500 independent runs. Note that the true and estimated Markov parameters of $\mathcal{T}_{2,1|1}$, $\mathcal{T}_{2,1|2}$, $\mathcal{T}_{3,2|1}$, and $\mathcal{T}_{3,2|2}$ are close to each other.

parameters are used in the EIV algorithm shown in Section 6 with $\epsilon = 10^{-8}$ to obtain the corrected Markov parameters.

Fig. 4 shows the Markov parameters of the transmissibilities $\mathcal{T}_{2,1|1}$, $\mathcal{T}_{2,1|2}$, $\mathcal{T}_{3,2|1}$, and $\mathcal{T}_{3,2|2}$, and the Markov parameters of the estimated transmissibilities $\hat{\mathcal{T}}_{2,1|1,r,d}$, $\hat{\mathcal{T}}_{2,1|2,r,d}$, $\hat{\mathcal{T}}_{3,2|1,r,d}$, and $\hat{\mathcal{T}}_{3,2|2,r,d}$, respectively, obtained using the EIV algorithm shown in Section 6. Note from Fig. 4 that the true and estimated Markov parameters of $\mathcal{T}_{2,1|1}$, $\mathcal{T}_{2,1|2}$, $\mathcal{T}_{3,2|1}$, and $\mathcal{T}_{3,2|2}$ are close to each other.

Next, we use ERA with $n_s = n_u = 5$ to construct the IIR models $\hat{\mathcal{T}}_{2,1|1}$, $\hat{\mathcal{T}}_{3,2|1}$, $\hat{\mathcal{T}}_{2,1|2}$, $\hat{\mathcal{T}}_{3,2|2}$ from the estimated transmissibilities $\hat{\mathcal{T}}_{2,1|1,r,d}$, $\hat{\mathcal{T}}_{3,2|1,r,d}$, $\hat{\mathcal{T}}_{2,1|2,r,d}$, $\hat{\mathcal{T}}_{3,2|2,r,d}$, respectively, where poles and zeros that are within a distance of 10^{-6} of each other are canceled. Next, the zeros of the estimated transmissibilities

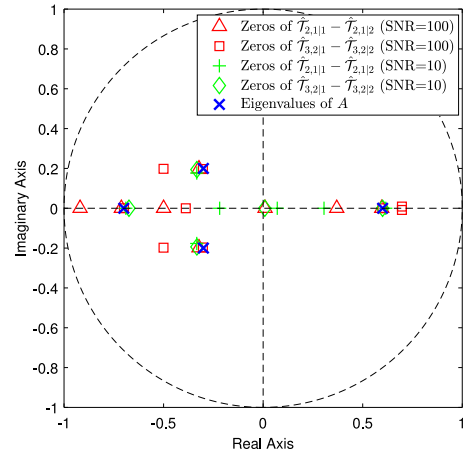


Fig. 5. Illustration of Theorem 1 using simulated noisy data. The eigenvalues of A given in (115) and the zeros of the estimated transmissibilities $\hat{\mathcal{T}}_{2,1|1} - \hat{\mathcal{T}}_{2,1|2}$ and $\hat{\mathcal{T}}_{3,2|1} - \hat{\mathcal{T}}_{3,2|2}$ are shown, where zero-mean white Gaussian noise is added to the output measurements y_1 , y_2 , and y_3 with SNR of 100 and 10. Note that all four eigenvalues of A are estimated correctly using $\hat{\mathcal{T}}_{2,1|1} - \hat{\mathcal{T}}_{2,1|2}$ and $\hat{\mathcal{T}}_{3,2|1} - \hat{\mathcal{T}}_{3,2|2}$, and the remaining zeros of $\hat{\mathcal{T}}_{2,1|1} - \hat{\mathcal{T}}_{2,1|2}$ and $\hat{\mathcal{T}}_{3,2|1} - \hat{\mathcal{T}}_{3,2|2}$ are spurious zeros due to noise.

$\hat{\mathcal{T}}_{2,1|1} - \hat{\mathcal{T}}_{2,1|2}$ and $\hat{\mathcal{T}}_{3,2|1} - \hat{\mathcal{T}}_{3,2|2}$ are obtained. Fig. 5 shows the eigenvalues of the A matrix given in (115) and the zeros of the estimated transmissibilities $\hat{\mathcal{T}}_{2,1|1} - \hat{\mathcal{T}}_{2,1|2}$ and $\hat{\mathcal{T}}_{3,2|1} - \hat{\mathcal{T}}_{3,2|2}$. Note that all eigenvalues of A are estimated correctly using $\hat{\mathcal{T}}_{2,1|1} - \hat{\mathcal{T}}_{2,1|2}$ and $\hat{\mathcal{T}}_{3,2|1} - \hat{\mathcal{T}}_{3,2|2}$, where the remaining zeros of $\hat{\mathcal{T}}_{2,1|1} - \hat{\mathcal{T}}_{2,1|2}$ and $\hat{\mathcal{T}}_{3,2|1} - \hat{\mathcal{T}}_{3,2|2}$ are spurious zeros due to noise. The results of the example confirm Theorem 1.

Next, we consider estimating the transfer functions $G_{i,j}$ from u_i to y_j , where $i = 1, 2, 3$ and $j = 1, 2$, and the denominator of these transfer functions is the polynomial constructed from the estimated eigenvalues of A shown in Fig. 5. Note that the numerator of the transfer function $G_{2,1}$, for example, is also the numerator of the transmissibility $\mathcal{T}_{2,1|1}$ and the denominator of the transmissibility $\mathcal{T}_{3,2|1}$. Similarly, we use the estimated transmissibilities to construct the numerators of the transfer functions $G_{i,j}$, where $i = 1, 2, 3$ and $j = 1, 2$, and to detect the spurious zeros. Finally, the estimated transfer functions are obtained by dividing the estimated numerators of the transfer function by the estimated denominators. Figs. 6 and 7 show the frequency response of the true and estimated transfer functions $G_{2,2}$ and $G_{3,2}$, respectively. Note from Figs. 6 and 7 that the frequency responses of the transfer function $G_{2,2}$ and $G_{3,2}$ are estimated correctly. \diamond

9. Experimental sensor-only estimation of the modal frequencies of an acoustic system

We consider the experimental setup shown in Fig. 8, which consists of an acoustic space with two speakers and three microphones. The speakers are the actuators that excite the acoustic space, and the microphones are the sensors that measure the acoustic response at their locations. The goal is to use sensor-only data to estimate the modal frequencies of the acoustic space. The sampling time used in the experiment is $T_s = 0.001$ s.

Let $\mathcal{T}_{j,ik}(\mathbf{q})$ denote the transmissibility whose pseudo input is the i th microphone and whose pseudo output is the j th microphone with excitation from the k th speaker. Moreover, let $\hat{\mathcal{T}}_{j,ik}(\mathbf{q}, \hat{\theta}_{r,d,l})$ denote an estimated noncausal CFI model of the transmissibility $\mathcal{T}_{j,ik}(\mathbf{q})$, where $\hat{\theta}_{r,d,l}$ is the vector of estimated denominator coefficients and Markov parameters obtained using least squares with a noncausal CFI model with orders r , d , and l

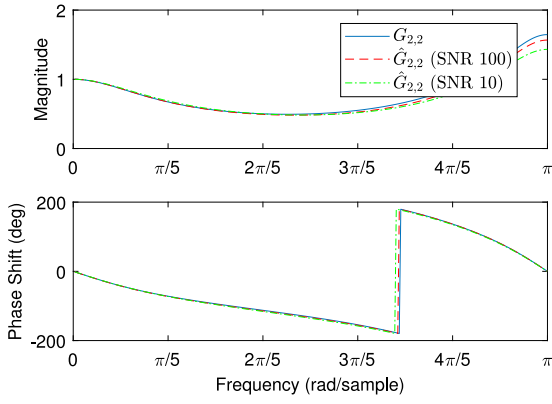


Fig. 6. Frequency response of the transfer function $G_{2,2}$ from u_2 to y_2 and the estimated transfer function $\hat{G}_{2,2}$ constructed from the estimated transmissibilities $\hat{\tau}_{2,1|1}$, $\hat{\tau}_{2,1|2}$, $\hat{\tau}_{3,2|1}$, $\hat{\tau}_{3,2|2}$ as shown in Section 5, where white, Gaussian noise with SNR's of 100 and 10 is added to the output measurements y_1 , y_2 , and y_3 . The denominator of $\hat{G}_{2,2}$ is constructed from the estimated eigenvalues of A shown in Fig. 5, where the numerator of $\hat{G}_{2,2}$ is constructed from the numerator of $\hat{\tau}_{2,1|2}$ and the denominator of $\hat{\tau}_{3,2|2}$. Note that the frequency response of the transfer function $G_{2,2}$ is estimated correctly.

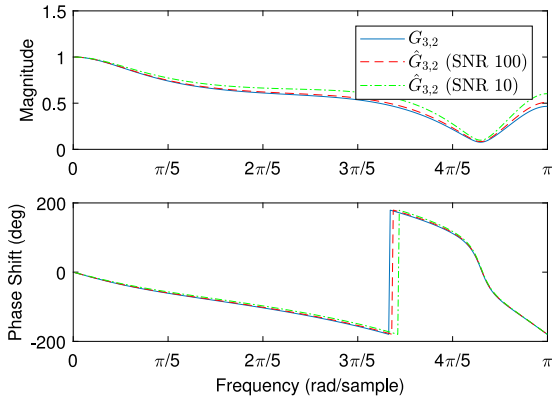


Fig. 7. Frequency response of the transfer function $G_{3,2}$ from u_2 to y_3 and the estimated transfer function $\hat{G}_{3,2}$ constructed from the estimated transmissibilities $\hat{\tau}_{2,1|1}$, $\hat{\tau}_{2,1|2}$, $\hat{\tau}_{3,2|1}$, $\hat{\tau}_{3,2|2}$ as shown in Section 5, where white, Gaussian noise with SNR's of 100 and 10 is added to the output measurements y_1 , y_2 , and y_3 . The denominator of $\hat{G}_{3,2}$ is constructed from the estimated eigenvalues of A shown in Fig. 5, where the numerator of $\hat{G}_{3,2}$ is constructed from the numerators of $\mathcal{T}_{3,1|2}$ and $\mathcal{T}_{3,2|2}$. Note that the frequency response of the transfer function $G_{3,2}$ is estimated correctly.

defined by (94) and where ℓ is the number of samples of each signal used for identification.

We first consider the case where Spk1 is operating and Spk2 is not operating. We obtain measurements from microphones Mic1–Mic3, and we use least squares with $\ell = 10,000$ samples to fit a noncausal CFI model with $l = 5$ and $r = d = 33$ in order to estimate the transmissibilities $\mathcal{T}_{2,1|1}$ and $\mathcal{T}_{3,2|1}$. Next, we consider the case where Spk2 is operating and Spk1 is not operating. We obtain measurements from the microphones Mic1, Mic2, and Mic3, and we use least squares with $\ell = 10,000$ samples to fit a noncausal CFI model with $l = 5$ and $r = d = 33$ in order to estimate the transmissibilities $\mathcal{T}_{2,1|2}$ and $\mathcal{T}_{3,2|2}$. Fig. 9 shows the Markov parameters and poles of the estimated noncausal CFI models of the transmissibilities $\hat{\tau}_{2,1|1}(\mathbf{q}, \hat{\theta}_{r,d,\ell})$ and $\hat{\tau}_{2,1|2}(\mathbf{q}, \hat{\theta}_{r,d,\ell})$. Moreover, Fig. 10 shows the Markov parameters



Fig. 8. Acoustic experiment setup. Two speakers and three microphones are used in the experiment to excite the three-dimensional acoustic space and measure its response.

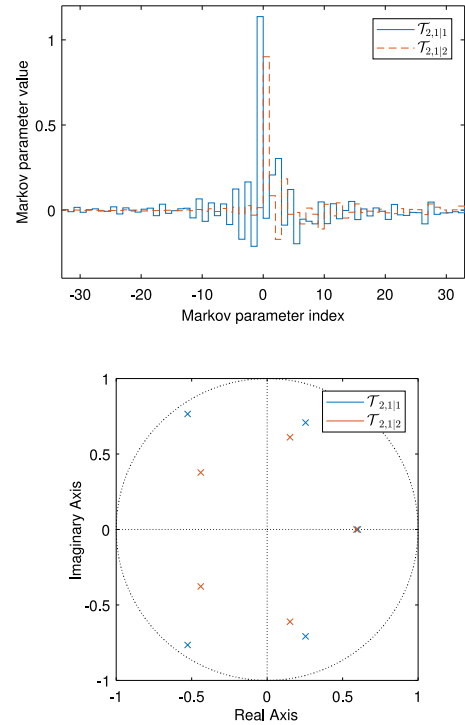


Fig. 9. Markov parameters and poles of the noncausal CFI models of the estimated transmissibilities $\mathcal{T}_{2,1|1}$ and $\mathcal{T}_{2,1|2}$.

and poles of the estimated noncausal CFI models of the transmissibilities $\hat{\tau}_{3,2|1}(\mathbf{q}, \hat{\theta}_{r,d,\ell})$ and $\hat{\tau}_{3,2|2}(\mathbf{q}, \hat{\theta}_{r,d,\ell})$.

Note from Figs. 9 and 10 that all four estimated transmissibilities $\hat{\tau}_{2,1|1}(\mathbf{q}, \hat{\theta}_{r,d,\ell})$, $\hat{\tau}_{2,1|2}(\mathbf{q}, \hat{\theta}_{r,d,\ell})$, $\hat{\tau}_{3,2|1}(\mathbf{q}, \hat{\theta}_{r,d,\ell})$, and $\hat{\tau}_{3,2|2}(\mathbf{q}, \hat{\theta}_{r,d,\ell})$ have both causal and noncausal components. Fig. 11 shows a comparison of the frequency responses of the estimated noncausal CFI models of the transmissibilities $\mathcal{T}_{2,1|1}$, $\mathcal{T}_{2,1|2}$, $\mathcal{T}_{3,2|1}$, and $\mathcal{T}_{3,2|2}$ with $l = 5$, $r = 33$, and $d = 33$ with the frequency response of the constructed IIR model with $n_s = 15$ and $n_u = 15$.

Next, we use ERA to construct state space realizations of the stable and unstable components of the estimated transmissibility models $\hat{\tau}_{2,1|1}(\mathbf{q}, \hat{\theta}_{r,d,\ell})$, $\hat{\tau}_{2,1|2}(\mathbf{q}, \hat{\theta}_{r,d,\ell})$, $\hat{\tau}_{3,2|1}(\mathbf{q}, \hat{\theta}_{r,d,\ell})$, and $\hat{\tau}_{3,2|2}(\mathbf{q}, \hat{\theta}_{r,d,\ell})$ with $n_s = 15$ and $n_u = 15$. We then cancel all

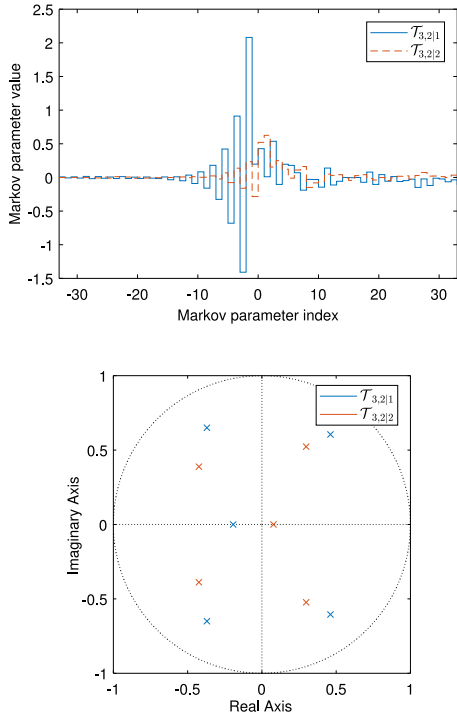


Fig. 10. Markov parameters and poles of the noncausal CFI models of the estimated transmissibilities $\mathcal{T}_{3,2|1}$ and $\mathcal{T}_{3,2|2}$.

pairs of poles and zeros of the estimated state space models of the transmissibilities $\hat{\mathcal{T}}_{2,1|1}(\mathbf{q}, \hat{\theta}_{r,d,\ell})$, $\hat{\mathcal{T}}_{2,1|2}(\mathbf{q}, \hat{\theta}_{r,d,\ell})$, $\hat{\mathcal{T}}_{3,2|1}(\mathbf{q}, \hat{\theta}_{r,d,\ell})$, and $\hat{\mathcal{T}}_{3,2|2}(\mathbf{q}, \hat{\theta}_{r,d,\ell})$ that are within a distance of 1×10^{-6} of each other.

Fig. 12 shows the pole-zero maps of the estimated state space models of the transmissibilities $\hat{\mathcal{T}}_{2,1|1}(\mathbf{q}, \hat{\theta}_{r,d,\ell})$, $\hat{\mathcal{T}}_{2,1|2}(\mathbf{q}, \hat{\theta}_{r,d,\ell})$, $\hat{\mathcal{T}}_{3,2|1}(\mathbf{q}, \hat{\theta}_{r,d,\ell})$, and $\hat{\mathcal{T}}_{3,2|2}(\mathbf{q}, \hat{\theta}_{r,d,\ell})$ after the pole-zero cancellation.

Next, we consider the differences of transmissibilities $\mathcal{T}_{2,1|1} - \mathcal{T}_{2,1|2}$ and $\mathcal{T}_{3,2|1} - \mathcal{T}_{3,2|2}$. It follows from Theorem 1 that the modal parameters of the acoustic system can be estimated from the zeros of $\mathcal{T}_{2,1|1} - \mathcal{T}_{2,1|2}$ and $\mathcal{T}_{3,2|1} - \mathcal{T}_{3,2|2}$.

For validation, the modal parameters of the acoustic system are directly estimated using measurements obtained from the speakers and microphones. To do this, we identify the transfer functions $G_{1,2}$ from Spk2 to Mic1 and $G_{2,2}$ from Spk2 to Mic2 using least squares with an IIR model of order $\hat{n} = 10$. Fig. 13 shows the estimated zeros of $\mathcal{T}_{2,1|1} - \mathcal{T}_{2,1|2}$ and $\mathcal{T}_{3,2|1} - \mathcal{T}_{3,2|2}$ as well as the estimated poles of $G_{1,2}$ and $G_{2,2}$. In particular, estimates of the modal frequencies of the acoustic system are obtained from the estimated zeros of $\mathcal{T}_{2,1|1} - \mathcal{T}_{2,1|2}$ and $\mathcal{T}_{3,2|1} - \mathcal{T}_{3,2|2}$, where the scattered poles and zeros are spurious due to noise. Fig. 13 shows that three pairs of poles of $G_{1,2}$ and $G_{2,2}$ are close to three pairs of zeros of $\mathcal{T}_{2,1|1} - \mathcal{T}_{2,1|2}$ and $\mathcal{T}_{3,2|1} - \mathcal{T}_{3,2|2}$. Table 1 shows the estimated modal frequencies and damping ratios obtained by identifying the transfer functions $G_{1,2}$ and $G_{2,2}$ directly and by the estimated transmissibilities $\mathcal{T}_{2,1|1} - \mathcal{T}_{2,1|2}$ and $\mathcal{T}_{3,2|1} - \mathcal{T}_{3,2|2}$. The average of the estimated modal frequencies and damping ratios are computed for both cases. In particular, the estimated modal frequencies of the system based on the identified transfer functions are $\omega_{n1} = 423.5$ rad/s, $\omega_{n2} = 785.1$ rad/s, and $\omega_{n3} = 2214.8$ rad/s, whereas the estimated modal frequencies of the system based on the transmissibilities and Theorem 1 are $\hat{\omega}_{n1} = 415.0$ rad/s, $\hat{\omega}_{n2} = 773.5$ rad/s, and $\hat{\omega}_{n3} = 2179.0$ rad/s. The errors in the estimates of ω_{n1} , ω_{n2} , and ω_{n3} are 2.0%, 1.5%, and 1.6%, respectively. Similarly, the estimated damping ratios of the three modes obtained from the identified

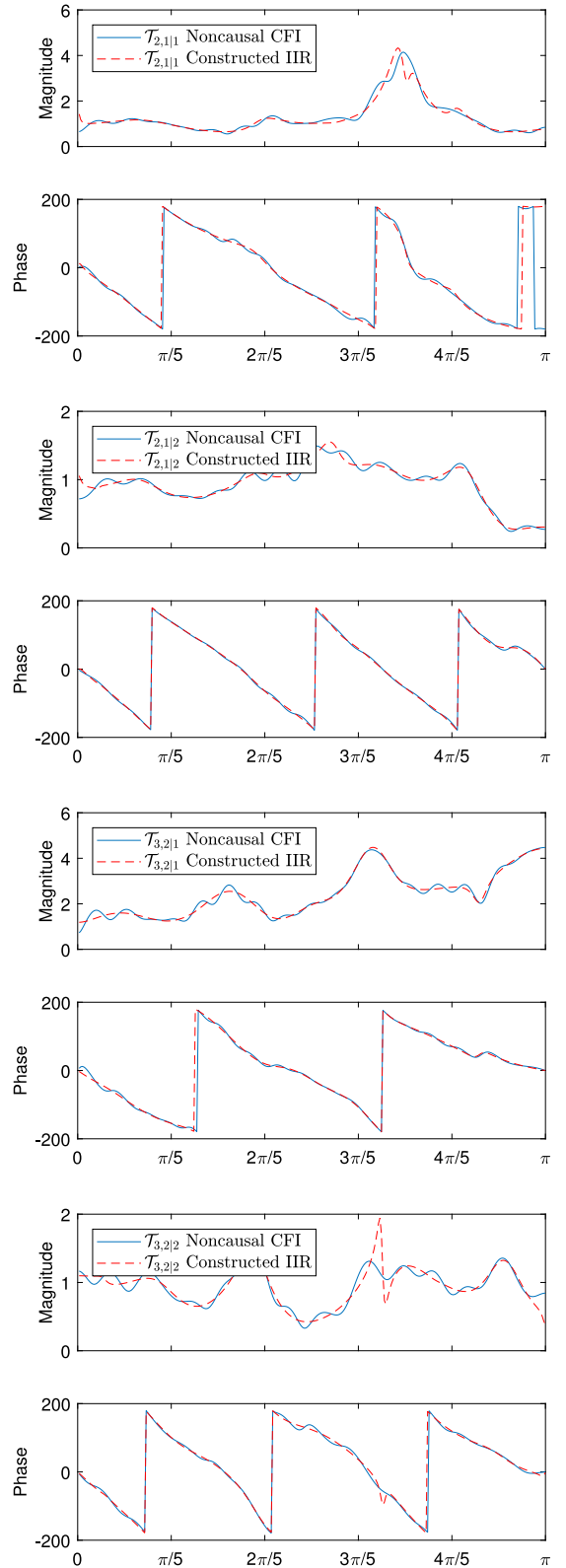


Fig. 11. Comparison of the frequency responses of the estimated noncausal CFI models of the transmissibilities $\mathcal{T}_{2,1|1}$, $\mathcal{T}_{2,1|2}$, $\mathcal{T}_{3,2|1}$, and $\mathcal{T}_{3,2|2}$ obtained with $l = 5$, $r = 33$, and $d = 33$ with the frequency responses of the constructed IIR models obtained with $n_s = 15$ and $n_u = 15$.

transfer functions are $\zeta_1 = 0.365$, $\zeta_2 = 0.19$, and $\zeta_3 = 0.12$, where the estimated damping ratios of the three modes obtained

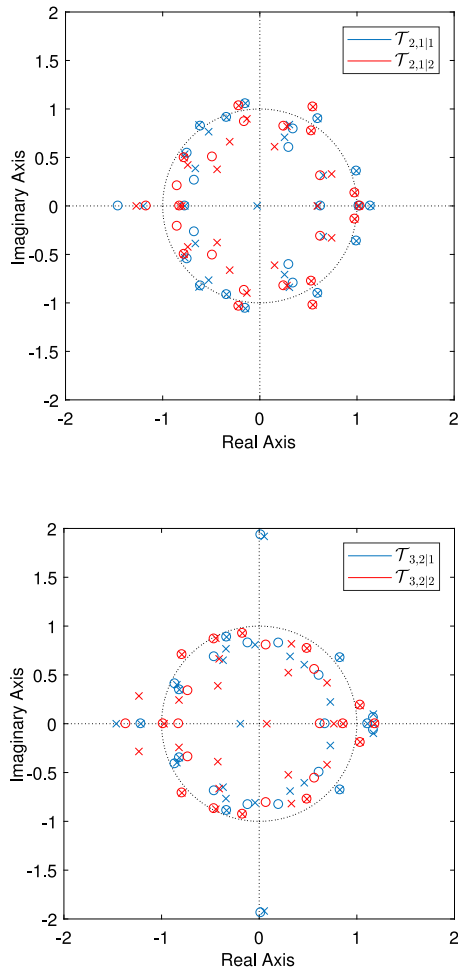


Fig. 12. Pole-zero maps of the estimated IIR models of the transmissibilities $\mathcal{T}_{2,1|1}$, $\mathcal{T}_{2,1|2}$, $\mathcal{T}_{3,2|1}$, and $\mathcal{T}_{3,2|2}$.

Table 1

Modal frequencies (in rad/s) and damping ratios estimated from the identified transfer functions $G_{1,2}$ and $G_{2,2}$ directly and from the estimated transmissibilities $\mathcal{T}_{2,1|1} - \mathcal{T}_{2,1|2}$ and $\mathcal{T}_{3,2|1} - \mathcal{T}_{3,2|2}$.

	ω_{n1}	ζ_1	ω_{n2}	ζ_2	ω_{n3}	ζ_3
$G_{1,2}$	441.7	0.37	787.3	0.16	2241.8	0.11
$G_{2,2}$	405.3	0.36	782.9	0.21	2187.8	0.13
Averaged	423.5	0.365	785.1	0.19	2214.8	0.12
$\mathcal{T}_{2,1 1} - \mathcal{T}_{2,1 2}$	383.9	0.47	789.2	0.24	2190.3	0.13
$\mathcal{T}_{3,2 1} - \mathcal{T}_{3,2 2}$	446.1	0.39	757.8	0.32	2167.7	0.16
Estimated	415.0	0.43	773.5	0.28	2179.0	0.15
Error (%)	2.0	16.2	1.5	47.3	1.6	25

from estimated transmissibilities are $\hat{\zeta}_1 = 0.43$, $\hat{\zeta}_2 = 0.28$, and $\hat{\zeta}_3 = 0.15$, which correspond to errors of 16.2%, 47.3%, and 25.0%, respectively. The large errors in the estimated damping ratios is due to the lack of an EIV algorithm for noncausal CFI models.

10. Conclusions

This paper introduced transmissibility-based system identification (TBSID), which is a time-domain technique for system identification that uses only output data. In particular, TBSID uses output data from a system driven by unknown and unspecified but sufficiently persistent inputs applied at distinct

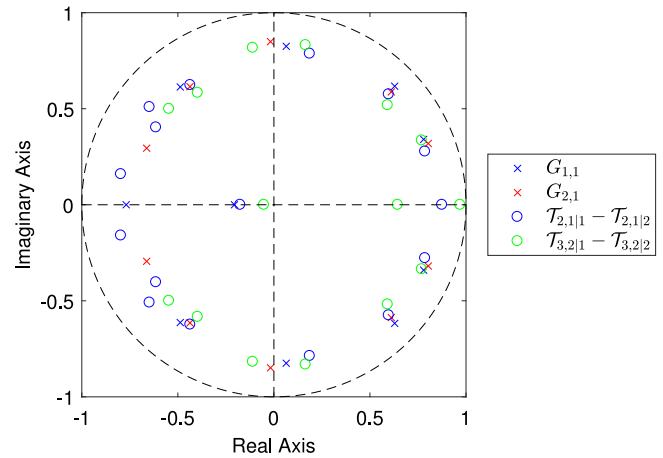


Fig. 13. Estimated poles of $G_{1,2}$ and $G_{2,2}$ obtained using least squares with an IIR model with order $n = 10$, and zeros of the estimated models of $\mathcal{T}_{2,1|1} - \mathcal{T}_{2,1|2}$ and $\mathcal{T}_{3,2|1} - \mathcal{T}_{3,2|2}$. Note that there are three pairs of estimated poles of $G_{1,2}$ and $G_{2,2}$ that are close to three pairs of estimated zeros of $\mathcal{T}_{2,1|1} - \mathcal{T}_{2,1|2}$ and $\mathcal{T}_{3,2|1} - \mathcal{T}_{3,2|2}$. The estimated modal frequencies of the acoustic system are obtained from the estimated zeros of $\mathcal{T}_{2,1|1} - \mathcal{T}_{2,1|2}$ and $\mathcal{T}_{3,2|1} - \mathcal{T}_{3,2|2}$ and compared to the estimated modal frequencies obtained from $G_{1,2}$ and $G_{2,2}$. The remaining poles and zeros, which are scattered over the unit disk, are spurious due to noise.

locations to estimate two transmissibility operators, which are then used to construct an input–output model. As in the case of frequency-domain transmissibility estimation (Devriendt & Guillaume, 2008; Weijtjens et al., 2014), the excitation must be applied nonsimultaneously at two different locations, and the identification method may produce spurious modes. The feasibility of TBSID was illustrated on numerical examples and demonstrated on an experimental acoustic application using noncausal composite FIR/IIR (CFI) models, where the three modal frequencies were estimated within 2%.

Further research will address the following challenges. First, systematic techniques are needed to detect and remove spurious modes. Next, the effect of sensor noise must be considered. Since sensor data are used to identify the transmissibilities, sensor noise leads to an errors-in-variables (EIV) problem (Söderström, 2018). In this case, the sensor noise may be colored but uncorrelated. The accuracy of TBSID may thus benefit from the availability of an effective EIV technique for noncausal CFI models. Finally, it can occur in practice that an additional input signal is applied at a different location concurrently with the unknown input signals. In this case, the sensor noise is colored and correlated, thus leading to a more challenging EIV problem.

References

- Abed-Meraim, K., Qiu, W., & Hua, Y. (1997). Blind system identification. *Proceedings of the IEEE*, 85(8), 1310–1322.
- Aljanaideh, K. F., & Bernstein, D. S. (2015a). Time-domain analysis of motion transmissibilities in force-driven and displacement-driven structures. *Journal of Sound and Vibration*, 347, 169–183.
- Aljanaideh, K. F., & Bernstein, D. S. (2015b). Time-domain analysis of sensor-to-sensor transmissibility operators. *Automatica*, 53, 312–319.
- Aljanaideh, K. F., & Bernstein, D. S. (2017a). A behavioral equation framework for time-domain transmissibilities. *Automatica*, 78, 20–24.
- Aljanaideh, K. F., & Bernstein, D. S. (2017b). Closed-loop identification of unstable systems using noncausal FIR models. *International Journal of Control*, 90(2), 168–185.
- Aljanaideh, K. F., & Bernstein, D. S. (2018a). Experimental application of time-domain transmissibility identification to fault detection and localization in acoustic systems. *Journal of Vibration and Acoustics*, 140, 021017-1–021017-11.
- Aljanaideh, K. F., & Bernstein, D. S. (2018b). Initial conditions in time- and frequency-domain system identification. *IEEE Control Systems Magazine*, 38, 80–93.

- Aljanaideh, K. F., & Bernstein, D. S. (2018c). Reconstruction of aircraft lateral dynamics using two transmissibility operators. In *IEEE conference on decision and control* (pp. 7153–7157). Miami Beach, FL.
- Aljanaideh, K. F., & Bernstein, D. S. (2018d). System identification using composite FIR/IIR models. In *American control conference* (pp. 5639–5644). Milwaukee, WI.
- Aljanaideh, K. F., Sanjeevini, S., & Bernstein, D. S. (2018). Time-domain errors-in-variables identification of transmissibilities. In *IEEE conference on decision and control* (pp. 3012–3017).
- Brincker, R., Zhang, L., & Andersen, P. (2001). Modal identification of output-only systems using frequency domain decomposition. *Smart Materials and Structures*, 10(3), 441.
- Brualdi, R. A., & Schneider, H. (1983). Determinantal identities: Gauss, schur, Cauchy, sylvester, kronecker, Jacobi, binet, Laplace, muir, and Cayley. *Linear Algebra and its Applications*, 52, 769–791.
- Devriendt, C., De Sitter, G., & Guillaume, P. (2010). An operational modal analysis approach based on parametrically identified multivariable transmissibilities. *Mechanical Systems and Signal Processing*, 24(5), 1250–1259.
- Devriendt, C., De Sitter, G., Vanlanduit, S., & Guillaume, P. (2009). Operational modal analysis in the presence of harmonic excitations by the use of transmissibility measurements. *Mechanical Systems and Signal Processing*, 23(3), 621–635.
- Devriendt, C., & Guillaume, P. (2007). The use of transmissibility measurements in output-only modal analysis. *Mechanical Systems and Signal Processing*, 21(7), 2689–2696.
- Devriendt, C., & Guillaume, P. (2008). Identification of modal parameters from transmissibility measurements. *Journal of Sound and Vibration*, 314(1–2), 343–356.
- Diversi, R. (2008). A bias-compensated identification approach for noisy FIR models. *IEEE Signal Processing Letters*, 15, 325–328.
- Ewins, D. J. (1984). *Modal testing: Theory and practice*. Letchworth.
- Ewins, D. J. (2000). Basics and state-of-the-art of modal testing. *Sadhana*, 25(3), 207–220.
- Eykhoff, P. (1974). *System identification: Parameter and state estimation*. Wiley.
- Hermans, L., & Van der Auweraer, H. (1999). Modal testing and analysis of structures under operational conditions: industrial applications. *Mechanical Systems and Signal Processing*, 13(2), 193–216.
- Juang, J. N. (1994). *Applied system identification*. Upper Saddle River, NJ: Prentice-Hall.
- Ljung, L. (1998). System identification. In *Signal analysis and prediction* (pp. 163–173). Springer.
- Lo, C., Lynch, J. P., & Liu, M. (2011). Reference-free detection of spike faults in wireless sensor networks. In *4th international symposium on resilient control systems* (pp. 148–153).
- Lo, C., Lynch, J. P., & Liu, M. (2012). Pair-wise reference-free fault detection in wireless sensor networks. In *Proceedings of the 11th international conference on information processing in sensor networks* (pp. 117–118).
- Lo, C., Lynch, J. P., & Liu, M. (2013). Distributed reference-free fault detection method for autonomous wireless sensor networks. *IEEE Sensors Journal*, 13(5), 2009–2019.
- Maamar, A., Abdelghani, M., Le, T.-P., Gagnol, V., & Sabourin, L. (2019). Operational modal identification in the presence of harmonic excitation. *Applied Acoustics*, 147, 64–71.
- Middleton, R. H., & Goodwin, G. C. (1990). *Digital control and estimation: A unified approach*. Prentice Hall.
- Moulines, E., Duhamel, P., Cardoso, J.-F., & Mayrargue, S. (1995). Subspace methods for the blind identification of multichannel FIR filters. *IEEE Transactions on Signal Processing*, 43(2), 516–525.
- Peeters, B., & De Roeck, G. (2001). Stochastic system identification for operational modal analysis: a review. *Journal of Dynamic Systems, Measurement, and Control*, 123(4), 659–667.
- Recht, B., Fazel, M., & Parrilo, P. A. (2010). Guaranteed minimum-rank solutions of linear matrix equations via nuclear norm minimization. *SIAM Review*, 52(3), 471–501.
- Smith, R. S. (2014). Frequency domain subspace identification using nuclear norm minimization and Hankel matrix realizations. *IEEE Transactions on Automatic Control*, 59(11), 2886–2896.
- Söderström, T. (2018). *Errors-in-variables methods in system identification*. Springer.
- Söderström, T., & Stoica, P. (1989). *System identification*. Prentice-Hall.
- Tong, L., Xu, G., & Kailath, T. (1994). Blind identification and equalization based on second-order statistics: a time domain approach. *IEEE Transactions on Information Theory*, 40(2), 340–349.
- Weijtens, W., De Sitter, G., Devriendt, C., & Guillaume, P. (2014). Operational modal parameter estimation of mimo systems using transmissibility functions. *Automatica*, 50(2), 559–564.
- Zhang, L., Wang, T., & Tamura, Y. (2010). A frequency-spatial domain decomposition (fsdd) method for operational modal analysis. *Mechanical Systems and Signal Processing*, 24(5), 1227–1239.



Khaled F. Aljanaideh received the B.Sc. degree in mechanical engineering (top of class) from Jordan University of Science and Technology, Irbid, Jordan in 2009. He also received the M.S.E. and M.Sc. degrees in aerospace engineering and applied mathematics and the Ph.D. degree in aerospace engineering all from the University of Michigan, Ann Arbor, in 2011, 2014, and 2015, respectively. He is currently an assistant professor in the Department of Aeronautical Engineering, Jordan University of Science and Technology. He was a postdoctoral research fellow in the Department of

Aerospace Engineering at the University of Michigan between 2015 and 2016, where he also was a part-time visiting assistant professor between 2017 and 2019. His current research interests are in system identification and fault detection for aerospace and mechanical systems.



Dennis S. Bernstein received the Sc.B. degree from Brown University and the Ph.D. degree from the University of Michigan in Ann Arbor, Michigan, where he is currently professor in the Aerospace Engineering Department. His interests are in identification, estimation, and control for aerospace applications. He is the author of *Scalar, Vector, and Matrix Mathematics*, published by Princeton University Press.